2

Acoustical Prerequisites

2.1 Introduction

The difficulty of the subject of sound propagation through the stochastic ocean owes much of its complexity to the fact that sound transmission in the ocean occurs in a waveguide. Sound waves are continuously refracted and diffracted by the sound channel and the waves are bounded on the edges by the sea floor and surface. Therefore, this chapter provides an overview of the basic ocean acoustics concepts of guided propagation that are needed as a foundation to understand transmission through the fluctuating ocean waveguide. The key propagation methodologies to be covered in this chapter include ray theory, the Born approximation, Feynman path integrals, and the method of normal modes. Most of the background information provided here will involve sound propagation concepts in a vertically stratified ocean, but an effort is made to present the fundamental range-dependent equations for each propagation methodology and to briefly discuss implications for acoustic scattering.

Those readers with a solid background in underwater acoustics may not find anything particularly new in this chapter, but studying the following material is encouraged to foster a familiarity with the notation and broad approach of the monograph. By necessity this is an abridged treatment of the subject of underwater acoustics, and the reader is referred to numerous quality texts dedicated to this subject (see, for example, Brekhovskikh and Lysanov, 1991; Frisk, 1994; Jensen et al., 1994; Munk et al., 1995; Katznelson et al., 2012).

2.2 Fundamental Equations of Hydrodynamics

For ocean sound propagation the fundamental hydrodynamic equations are the continuity equation (conservation of mass), the momentum equation (Newton's Law), and the adiabatic equation of state (pressure as a function of density and

entropy). These are written

$$\frac{\partial \rho'}{\partial t} = -\nabla \cdot (\rho' \mathbf{u}'), \tag{2.1}$$

$$\rho' \left(\frac{\partial \mathbf{u}'}{\partial t} + \mathbf{u}' \cdot \nabla \mathbf{u}' \right) = -\nabla p', \tag{2.2}$$

$$p' = p'(\rho', s = \text{const.}), \tag{2.3}$$

where p' is the pressure, ρ' is the density, $\mathbf{u}'$ is the fluid velocity, and in the equation of state changes in pressure and density involve no heat conduction, that is, entropy (s) following a water parcel is constant (e.g., $\partial s/\partial t + \mathbf{u}' \cdot \nabla s$=0). Because most ocean acoustic problems involve propagation over many wavelengths, nonlinear effects are small. Further assuming a fluid otherwise at rest and expanding the pressure, density and entropy fields about a time independent state $p_0(\mathbf{r})$, $\rho_0(\mathbf{r})$, and $s_0(\mathbf{r})$ the following linearized acoustic equations are obtained:

$$\frac{\partial \rho}{\partial t} = -\rho_0 \nabla \cdot \mathbf{u}, \tag{2.4}$$

$$\rho_0 \frac{\partial \mathbf{u}}{\partial t} = -\nabla p, \tag{2.5}$$

$$p = \rho c^2, \tag{2.6}$$

where the acoustic quantities are now p, ρ, $\mathbf{u}$, and the speed of sound is given by the thermodynamic relation $c^{-2} = (\partial \rho_0/\partial p_0)_{s=\text{const}}$. A little manipulation of these equations leads to the acoustic wave equation (Pierce, 1994):

$$\frac{1}{c^2} \frac{\partial^2 p}{\partial t^2} = \rho_0 \nabla \cdot \left(\frac{1}{\rho_0} \nabla p \right). \tag{2.7}$$

Here the sound speed and density fields are dictated by the ocean fields of potential temperature θ, salinity S, and pressure p_0. The fluctuation of these ocean fields include the effects of internal waves (more later). In this derivation the time dependence of the ocean has been ignored. Because the speed of sound (~1500 m/s) is so much larger than the typical speeds of ocean processes (order cm/s) this "frozen medium" approximation is well justified. Taking into account background currents $\mathbf{U}$, the acoustic wave equation becomes (Pierce, 1994)

$$\frac{1}{c^2} \frac{D^2 p}{Dt^2} = \rho_0 \nabla \left(\frac{1}{\rho_0} \nabla p \right), \tag{2.8}$$

where $D/Dt = \partial/\partial t + \mathbf{U} \cdot \nabla$, and it is understood that this advection current may include the effects of internal waves. A comparison between the magnitude of internal wave terms in Eq. 2.8, that is $\delta c/c_0$, $|\mathbf{U}|/c_0$, and $\delta\rho/\rho$, reveals that the

flow and density field terms are respectively one and two orders of magnitude smaller than the sound-speed term (Flatté et al., 1979). Thus the density effect is completely ignored in the treatment of sound propagation and the current effect is generally considered only when treating reciprocal transmissions where signals are sent in opposite directions thereby canceling the large sound-speed term and leaving the smaller current effect.

2.2.1 Parabolic Wave Equation

The parabolic approximation has played an important role in the development of the subject of sound propagation through the stochastic ocean not only through the area of numerical simulation (Flatté and Tappert, 1975; Colosi et al., 1994) but also in the theoretical development associated with Feynman path integrals (Flatté et al., 1979). Thus some time is spent on this topic here and further development is given in Chapter 7.

If density variations and background flow fields are ignored then the standard wave equation is obtained, that is, $\partial^2 p/\partial t^2 = c^2 \nabla^2 p$. Examining a single-frequency ω such that $p = \Psi e^{-i\omega t}$, the wave equation becomes the Helmholtz equation:

$$\nabla^2 \Psi + \frac{\omega^2}{c^2} \Psi = 0. \tag{2.9}$$

Physically the parabolic approximation involves examining waves that move primarily in one direction, that is, in a small range of angles centered around a primary direction. Mathematically this preferred direction is chosen to be along the x-axis where it is useful to define $\Psi(\mathbf{r}) = A(\mathbf{r}) e^{iq_0 x}$, with $q_0 = \omega/c_0$ a reference wavenumber. Plugging this form into the Helmholtz equation then gives

$$\frac{\partial^2 A}{\partial x^2} + \frac{\partial^2 A}{\partial y^2} + \frac{\partial^2 A}{\partial z^2} + 2iq_0 \frac{\partial A}{\partial x} + \left(\frac{\omega^2}{c^2} - q_0^2 \right) A = 0. \tag{2.10}$$

Qualitatively, considering the amplitude function A to be a slowly varying function of x compared to the phase function $e^{iq_0 x}$, then this gives $\partial^2 A/\partial x^2 << 2iq_0 \partial A/\partial x$ with the result that

$$\frac{i}{q_0} \frac{\partial A}{\partial x} = -\frac{1}{2q_0^2} \left(\frac{\partial^2 A}{\partial y^2} + \frac{\partial^2 A}{\partial z^2} \right) + V(\mathbf{r}) A, \tag{2.11}$$

where $V(\mathbf{r}) = (1 - c_0^2/c^2(\mathbf{r}))/2$. Equation 2.11 is the parabolic equation. It has the same form as the Schrödinger wave equation in which the x-coordinate is substituted for the time coordinate, and $q_0 = 1/\hbar$ ($\hbar$ is Planck's constant) for a unit mass particle (Flatté, 1986). The analogy between quantum and acoustic systems has been quite fruitful because many of the tools that have been developed for quantum systems can be directly applied to underwater acoustics (e.g., Feynman

path integrals, time independent and dependent perturbation theory, and classical and quantum chaos). However with the correspondence between q_0 and Planck's constant, it is apparent that there is no quantum analogy to transient acoustic fields because these are characterized by a distribution of wavenumbers q_0.

The derivation can be a bit more rigorous, providing some additional insight. Using operator notation, define

$$P = \frac{\partial}{\partial x}, \quad \text{and} \quad Q = \left(1 - 2V(\mathbf{r}) + \frac{1}{q_0^2}\left(\frac{\partial^2}{\partial y^2} + \frac{\partial^2}{\partial z^2}\right)\right)^{1/2}, \tag{2.12}$$

and using these expressions, Eq. 2.10 becomes

$$\Big(P + iq_0(1-Q)\Big)\Big(P + iq_0(1+Q)\Big)A - iq_0[PQ - QP]A = 0. \tag{2.13}$$

Here the first term corresponds to the product of an outgoing $(1-Q)$ and incoming wave $(1+Q)$. Further, the last term is identically zero for $U = U(z)$, and for $(1/\omega)dc/dx << 1$ the term is negligible. Thus only keeping the outgoing wave, the one-way wave equation is obtained (Jensen et al., 1994):

$$\frac{\partial A}{\partial x} = iq_0\left[\left(1 - 2V(\mathbf{r}) + \frac{1}{q_0^2}\left(\frac{\partial^2}{\partial y^2} + \frac{\partial^2}{\partial z^2}\right)\right)^{1/2} - 1\right]A. \tag{2.14}$$

The parabolic equation results from Taylor expanding such that $Q = (1+\epsilon)^{1/2} \simeq 1 + \epsilon/2$ (i.e., small-angle approximation) giving Eq. 2.11 as before. Higher order, wide-angle approximations to Eq. 2.14 are quite commonly used in ocean acoustic numerical analysis and are discussed in detail in other textbooks (see Jensen et al., 1994).

2.3 Character of the Oceanic Acoustic Waveguide

As previously mentioned, one of the most striking aspects of sound propagation in the ocean is the effect of the vertical acoustic waveguide. Sound waves propagate due to the compressibility of sea water, and in the ocean, like in the atmosphere, this is an adiabatic not isothermal process, meaning there is no heat conduction during the passage of the wave. The thermodynamic relation gives the sound-speed equation,

$$\frac{1}{c^2} = \left(\frac{\partial \rho_0(p_0, \theta, S)}{\partial p_0}\right), \tag{2.15}$$

where $\rho_0(p_0, \theta, S)$ is the adiabatic equation of state, that is density as a function of pressure, p_0, potential temperature, θ, and salinity S. Potential temperature of a parcel of water is defined as the temperature that parcel would acquire if it

were brought adiabatically from some in situ pressure p and temperature T to a reference pressure p_{ref} (Gill, 1982). In oceanographic cases the reference pressure is typically taken to be at the ocean surface, $p_{ref} = 0$ decibars.

A simple empirical equation for sound speed due to Medwin and Clay (1997) in terms of in situ temperature (T in °C), depth (z in m), and salinity (S in ppth) is

$$c(T,S,z) = 1449.2 + 4.6T - 0.055T^2 + 0.00029T^3 + (1.34 - 0.01T)(S - 35) + 0.016z. \tag{2.16}$$

Sound speed is seen to increase with increases in all three of the dependent variables, but the sensitivity to salinity is rather weak compared to the others. Sound-speed equations used in practice are similar to Eq. 2.16 except the polynomial expansions include many more terms (e.g., DelGrosso, 1974; MacKenzie, 1981) .

The vertical gradient of sound speed is the largest gradient in the ocean and it has three terms, namely

$$\frac{dc}{dz} = \left(\frac{\partial c}{\partial \theta}\right)_{p_0,S} \frac{d\theta}{dz} + \left(\frac{\partial c}{\partial S}\right)_{p_0,\theta} \frac{dS}{dz} + \left(\frac{\partial c}{\partial p_0}\right)_{\theta,S} \frac{dp_0}{dz}. \tag{2.17}$$

The first two terms constitute the potential sound-speed gradient because a parcel of water is being followed at fixed pressure. These terms are critical for modulating internal-wave-induced sound-speed fluctuations because of the adiabaticity of internal-wave displacements (see Section 2.3.2). The potential sound-speed gradient is then written

$$\left(\frac{dc}{dz}\right)_p = \left(\frac{\partial c}{\partial \theta}\right)_{p_0,S} \frac{d\theta}{dz} + \left(\frac{\partial c}{\partial S}\right)_{p_0,\theta} \frac{dS}{dz}. \tag{2.18}$$

The third term is called the adiabatic gradient because this is the change in sound speed that would be obtained with fixed θ and S, and a change in pressure with no heat conduction. The adiabatic sound-speed gradient is thus written

$$\left(\frac{dc}{dz}\right)_a = \left(\frac{\partial c}{\partial p_0}\right)_{\theta,S} \frac{dp_0}{dz} = -\rho_0 g \left(\frac{\partial c}{\partial p_0}\right)_{\theta,S} = -c\gamma_a, \tag{2.19}$$

where the hydrostatic equation $dp_0/dz = -\rho_0 g$ has been used. In the deep ocean where the temperature and salinity gradients are small, the sound-speed profile will be largely adiabatic. The quantity γ_a defined in the last line of Eq. 2.19 will be used extensively and has a value of 0.0113 km^{-1} with little variability, except in high latitudes.

A closely related quantity which is important for both acoustics and internal waves is the vertical gradient of density, which is written

$$\frac{d\rho_0}{dz} = \left(\frac{\partial \rho_0}{\partial \theta}\right)_{p_0,S} \frac{d\theta}{dz} + \left(\frac{\partial \rho_0}{\partial S}\right)_{p_0,\theta} \frac{dS}{dz} + \left(\frac{\partial \rho_0}{\partial p_0}\right)_{\theta,S} \frac{dp_0}{dz}. \tag{2.20}$$

As in Eq. 2.17 the first two terms represent the potential gradient of density and the third term is the adiabatic gradient, which can be written using Eq. 2.15:

$$\left(\frac{d\rho_0}{dz}\right)_a = -\frac{\rho_0 g}{c^2}. \tag{2.21}$$

Because parcels of water displaced vertically in the ocean do so adiabatically it is the potential gradient of density that establishes the static stability of the water column (Gill, 1982). This stability quantity is conventionally expressed in terms of the buoyancy or Brunt-Väisälä frequency, whose square is written

$$N^2 = -\frac{g}{\rho}\left[\left(\frac{\partial\rho_0}{\partial\theta}\right)_{p_0,S}\frac{d\theta}{dz} + \left(\frac{\partial\rho_0}{\partial S}\right)_{p_0,\theta}\frac{dS}{dz}\right] = -\frac{g}{\rho}\left[\frac{d\rho_0}{dz} + \frac{g\rho_0}{c^2}\right], \tag{2.22}$$

where $\rho = \rho(p, T, S)$ is the in situ density. The water column will be statically stable if $N^2 > 0$. The buoyancy frequency squared is proportional to the potential gradient of density, which is the actual density gradient minus the adiabatic gradient.

2.3.1 Canonical Sound-Speed Profiles

Empirical numerical relations are used to compute sound speed from profiles of temperature, salinity, and depth. However, there exists a useful canonical relation (Munk, 1974). For the case in which there is approximately a linear temperature–salinity relation over all depth,

$$\frac{d\theta}{dz} = \frac{1}{a}\frac{dS}{dz}, \tag{2.23}$$

then the total sound-speed gradient can be related to the ocean stratification, namely

$$\frac{dc}{dz} = c\Big(GN^2(z) - \gamma_a\Big). \tag{2.24}$$

Here the constant G is given by

$$G = \frac{\frac{1}{c}\left(\frac{\partial c}{\partial\theta} + a\frac{\partial c}{\partial S}\right)}{-\frac{g}{\rho_0}\left(\frac{\partial\rho_0}{\partial\theta} + a\frac{\partial\rho_0}{\partial S}\right)}, \tag{2.25}$$

and it is expressible in terms of "typical" coefficients of thermal expansion, haline contraction, and thermal and saline effects on sound speed (Munk, 1974). Some of these values are given by

$$\begin{aligned} \frac{1}{c}\frac{\partial c}{\partial\theta} &\simeq 2.0\times10^{-3}\ ^\circ\mathrm{C}^{-1}, \frac{1}{\rho_0}\frac{\partial\rho_0}{\partial\theta} \simeq -0.25\times10^{-3}\ ^\circ\mathrm{C}^{-1}, \\ \frac{1}{c}\frac{\partial c}{\partial S} &\simeq 0.74\times10^{-3}\mathrm{PSU}^{-1}, \frac{1}{\rho_0}\frac{\partial\rho_0}{\partial S} \simeq 0.75\times10^{-3}\mathrm{PSU}^{-1}. \end{aligned} \tag{2.26}$$

The value of a for the linear temperature–salinity equation can be derived from the Turner Number, Tu, which gives the relative contributions of salinity and potential temperature to water column stability (Turner, 1979), that is

$$Tu = -\frac{\frac{1}{\rho_0}\frac{\partial \rho_0}{\partial S}\frac{dS}{dz}}{\frac{1}{\rho_0}\frac{\partial \rho_0}{\partial \theta}\frac{d\theta}{dz}}. \tag{2.27}$$

For North Pacific Intermediate waters it is found $Tu \simeq -0.3$, and near Bermuda at shallow depth $Tu \simeq 0.8$ (Munk, 1974). Mid-latitude values of G range from 1 to 3.

If one further assumes an exponentially stratified ocean, that is $N(z) = N_0 \exp(z/B)$, then Eq. 2.24 can be solved yielding

$$c(z) = c_A\left[1 + \frac{\gamma_a B}{2}\left(\mathrm{e}^{2(z-z_A)/B} - \frac{2(z-z_A)}{B} - 1\right)\right], \tag{2.28}$$

where c_A is the sound speed on the channel axis z_A. Equation 2.28 is called the canonical sound-speed profile, and values typical of a mid-latitude location are c_A = 1500 m/s and $B = z_A$=1000 m. The Munk profile will be used extensively in this monograph, for example, calculations in deep-water, mid-latitude environments.

In high latitudes the thermocline essentially disappears, leaving a nearly uniform temperature water column. In the absence of thermal effects the high-latitude ocean stratification is often supported by a halocline in the upper few hundred meters of the water. Thus in this instance there is some utility in a canonical polar profile (Munk et al., 1995) which is given by

$$c(z) = c_A\left[1 + \gamma_a z + \frac{\delta c}{c_A}(1 - \mathrm{e}^{-z/\hat{B}})\right]. \tag{2.29}$$

Here c_A is the sound speed at the surface, and in addition to the constant adiabatic sound-speed gradient (γ_a), the third term gives a nonadiabatic sound speed contribution in the upper ocean. Typical values are $c_A \simeq 1440$ m/s[1], $\delta c \simeq 15$ m/s and $\hat{B} \simeq 150$ m.

For shallow water there is quite a lot of variability in the background profile due to the multitude of processes that can come into play in this region. These include mixing events that occur at both the ocean boundaries, shelf break front meanders and front tidal advection, slope effects, and river outflow. However, a canonical form that can be fit readily to observations is of the form

$$c(z) = c_0 + \delta c\left(1 + \tanh\left(\frac{z - z_0}{\Delta}\right)\right) + (\overline{dc/dz})z, \tag{2.30}$$

[1] This surface sound-speed value is consistent with Eq. 2.16, since typical upper ocean Arctic temperatures are less than 0°C.

where δc, z_0, and Δ physically represent the sound speed anomaly, the location, and width of the thermocline, and $\overline{dc/dz}$ represents a mean sound-speed gradient. This mean gradient is often related to the foot of the shelf break front pushing up onto the continental shelf.

2.3.2 Sound-Speed Fluctuations due to Internal Waves

The primary effect of internal waves on the ocean sound-speed field is due to distortions of the background vertical profile from vertical displacements of density surfaces, $\zeta(\mathbf{r},t)$. Adding vertical displacements to an otherwise stratified ocean gives

$$c(z+\zeta(\mathbf{r},t)) \simeq c(z) + \left(\frac{dc}{dz}\right)_p \zeta(\mathbf{r},t) + \cdots, \tag{2.31}$$

where the potential sound-speed gradient is important here (total sound-speed gradient minus the adiabatic gradient) because of the adiabaticity of the internal-wave displacements, that is, no heat conduction occurs when an internal wave moves a water parcel vertically (Munk and Zachariasen, 1976). The second term in this Taylor expansion thus defines the internal-wave-induced sound-speed perturbation that will enter many calculations, namely,

$$\delta c(\mathbf{r},t) = \left(\frac{dc(z)}{dz}\right)_p \zeta(\mathbf{r},t). \tag{2.32}$$

It should be noted that in much of the literature, the potential sound-speed gradient component of Eq. 2.24 is often used in Eq. 2.32 to model internal-wave sound-speed perturbations, but a more proper treatment is to compute the potential sound-speed gradient directly from profiles of potential temperature and salinity.[2]

2.3.3 Example Profiles

Figures 2.1–2.3 show example vertical profiles of many acoustically relevant oceanographic quantities for mid-latitude, high-latitude, and continental shelf regions. For the mid-latitude case (Figure 2.1), the broad thermocline and relatively weak salinity variation give rise to a deep sound-channel axis at a depth somewhat less than 1000 m. This sound-speed profile is not unlike the Munk Canonical profile (Eq. 2.28), which is also plotted in the figure. The potential density and corresponding buoyancy frequency profiles are also not unlike the canonical exponential form. Lastly, the potential sound-speed gradient is seen to be largest in the upper ocean and essentially zero in the deep ocean. Because of Eq. 2.32 it is seen that the upper ocean will be the location where the largest sound-speed fluctuations from internal waves will occur.

[2] In practice the potential sound-speed gradient is computed using $(dc/dz)_p = dc(p_{ref}, \theta(z), S(z))/dz$, where one generally chooses $p_{ref} = 0$ decibars.

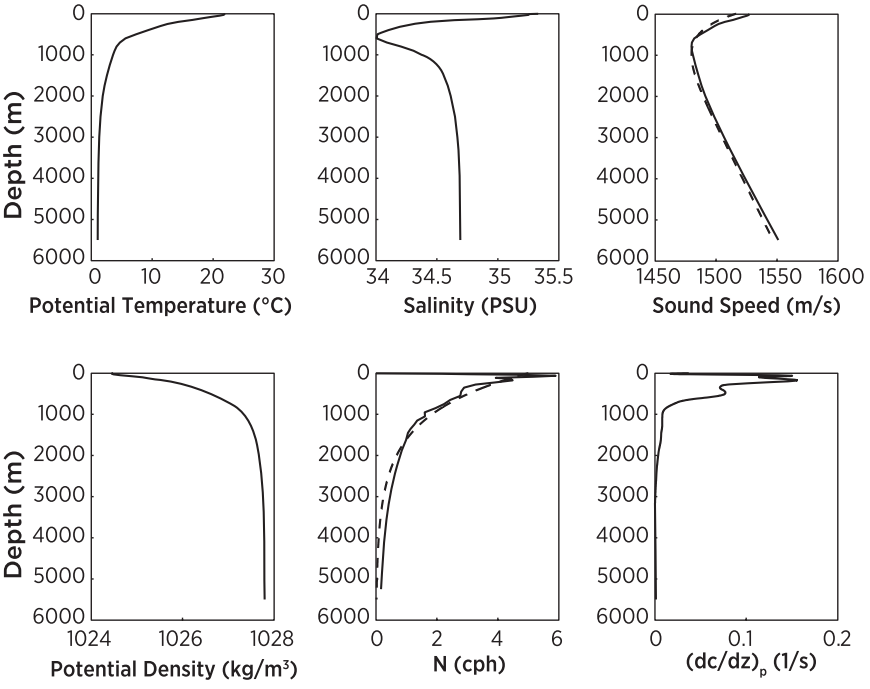

Figure 2.1. Examples of mid-latitude profiles of potential temperature, salinity, sound-speed, potential density, buoyancy frequency, and potential sound-speed gradient from the annual average World Ocean Atlas (Antonov et al., 2006; Locarnini et al., 2006). The profiles were taken from the location 30° N latitude, 150° W longitude. In the sound-speed panel the Munk canonical profile is plotted (dash, Eq. 2.28) for comparison, and in the buoyancy frequency panel an exponential profile $N(z) = 5\exp(z/1000)$ is plotted (dash) for comparison.

A typical high-latitude environment is depicted in Figure 2.2. Here the temperature is essentially uniform with depth, and there is a strong halocline in the upper ocean. The upper Arctic ocean is strongly freshened by significant river outflow. The resulting sound-speed profile is nearly linear (Eq. 2.29) with slope dictated by the adiabatic gradient. In the upper ocean there is a significant halocline effect on the sound-speed profile. The density and buoyancy frequency profiles reveal little stratification except in the halocline. The corresponding potential sound-speed gradient is small indeed relative to the mid-latitude case, meaning that an equal internal-wave displacement at mid-latitude and high latitude will result in a smaller sound-speed anomaly at high latitude. Internal waves are known to be quite weak in the high latitudes (see Chapter 3), so it is expected that acoustic fluctuations from these waves will be rather less important in this region. This situation may change as Arctic ice continues to diminish.

Figure 2.3 shows a typical summer continental shelf profile. The continental shelf has strong seasonal variability as storms can often mix the water column from top to bottom. In the example here there are both strong temperature and salinity

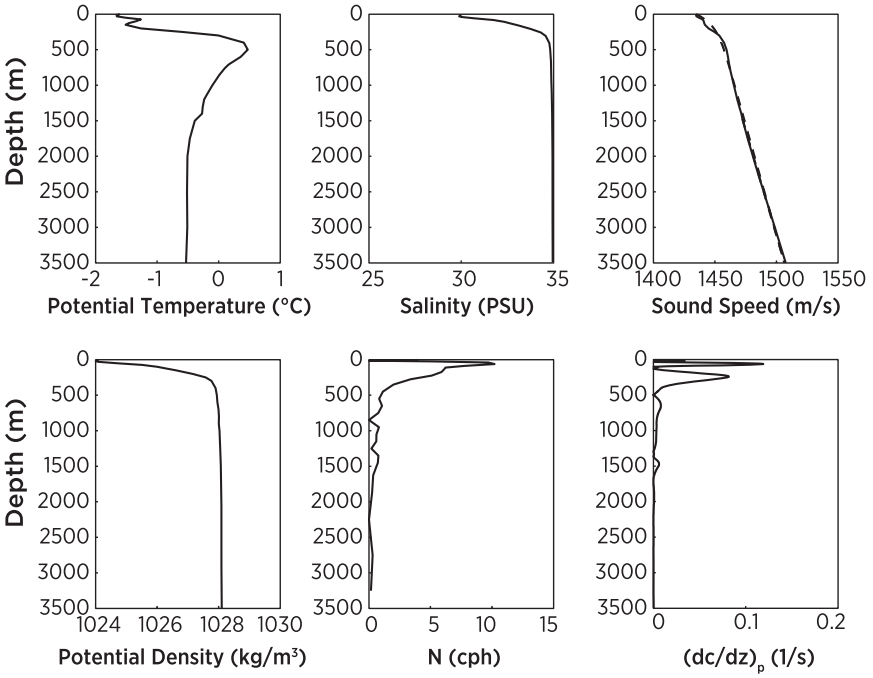

Figure 2.2. Profiles of potential temperature, salinity, sound speed, potential density, buoyancy frequency, and potential sound-speed gradient from the annual average World Ocean Atlas (Antonov et al., 2006; Locarnini et al., 2006). The profiles were taken from the location 80° N latitude, 150° W longitude. In the sound-speed panel a canonical Arctic profile (dash, Eq. 2.29) is shown for comparison.

gradients throughout the water column, resulting in a sound channel axis near 20-m depth. Here a canonical sound-speed profile based on Eq. 2.30 is plotted with the observation, where the parameters are: $c_0 = 1480$ m/s, $\delta c = 25$ m/s, $\Delta = 8$ m, $z_0 = 10$ m, and $\overline{dc/dz} = 0.3$ 1/s. The potential density profile varies rapidly though the strong thermocline, yielding extremely large values of the buoyancy frequency in the upper ocean. The potential sound-speed gradient is large in this case with peak values of order 100 and 10 times the high-latitude and mid-latitude values, respectively.

The interested reader can also refer to the ocean acoustic propagation atlas within the monograph Munk et al. (1995), which shows deep-water sound-speed profiles from around the world's oceans.

2.3.4 Attenuation of Sound

The attenuation of sound from seawater is generally quite small, and this fact is one of the most compelling ones in support of acoustic methodologies for remote sensing, navigation, and communication. But small is not zero, and much effort

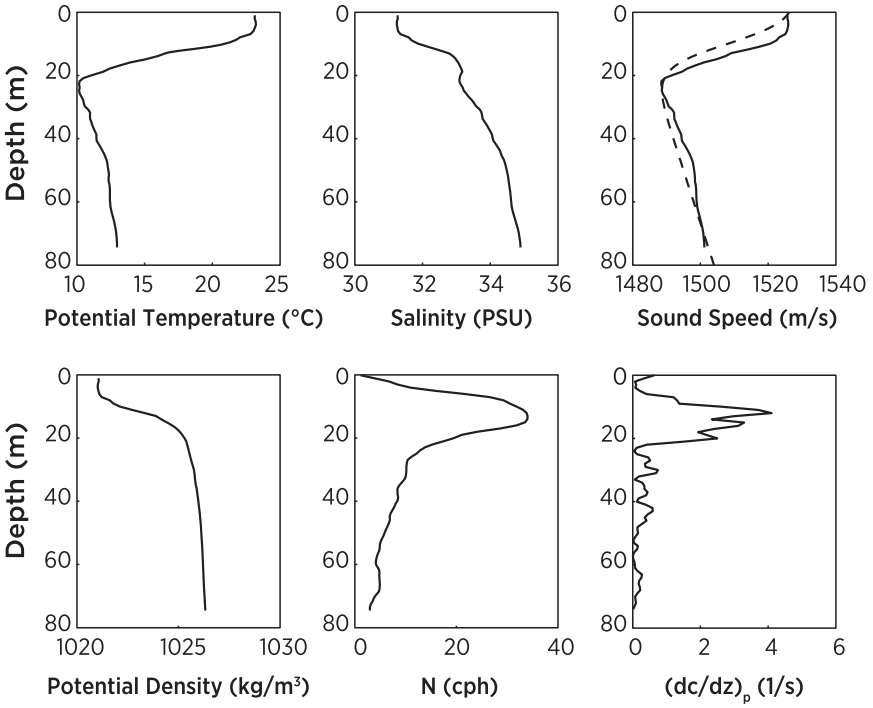

Figure 2.3. Profiles of potential temperature, salinity, sound speed, potential density, buoyancy frequency, and potential sound-speed gradient from measurements taken on the New Jersey continental shelf (Colosi et al., 2012). The profiles come from CTD data in the vicinity of 39° N latitude, 73° W longitude. A canonical sound-speed profile (dash) derived from Eq. 2.30 is shown with the observed sound-speed profile.

has been put toward formulating useful expressions for acoustic attenuation from seawater. Ocean acousticians choose to represent sound attenuation in many ways. The representation used here is to consider the acoustic wavenumber to have a small complex component, that is, the wavenumber is written $\omega/c + i\alpha$. Thus over one meter the relative change in acoustic amplitude is $e^{-\alpha(x+1)}/e^{-\alpha x} = e^{-\alpha}$. Written in units of dB/km the result is

$$\alpha'(\text{dB/km}) = 1000 \times (20 \log_{10} e^{\alpha}) \simeq 8686\, \alpha. \tag{2.33}$$

In this book the quantity α will generally be used for theoretical calculations, but tabulations of attenuation are generally given in terms of α', so the translation given above is quite practical.

A useful approximate expression for α' is (Thorpe, 1967; Fisher and Simmons, 1977; Urick, 1979)

$$\alpha' \simeq 3.3 \times 10^{-3} + 0.79A \frac{f^2}{(0.8)^2 + f^2} + \frac{36 f^2}{5000 + f^2} + 3.0 \times 10^{-4} f^2 \quad \text{dB/km}, \tag{2.34}$$

Table 2.1. *Geoacoustic properties of common marine sediments and seafloors*

Bottom type	Density (kg/m^3)	Sound speed (m/s)	Attenuation (dB/λ)[a]
Sand coarse	2034	1836	0.87
Sand medium	2014	1765	0.88
Sand fine	1962	1759	0.89
Sand very fine	1878	1709	1.05
Silty sand	1783	1658	1.13
Sandy silt	1769	1644	1.22
Silt	1740	1615	0.38
Sand-silt-clay	1575	1582	0.17
Clayey-silt	1489	1546	0.11
Silty-clay	1480	1517	0.08
Clay-mud	1312	1470	0.09
Chalk	2200	2400	0.2
Sandstone	2400	4350	0.1
Basalt	2550	4750	0.1
Granite	2650	5750	0.1
Limestone	2700	5350	0.1

[a]The unit dB/λ is converted to dB/m by dividing by m/λ.
Values shown are representative of natural conditions, and variations will occur site to site. Values based on Clay and Medwin (1977), Hamilton (1980), Hamilton (1987), Jensen et al. (1994), Buckingham (2005), APL-UW (2008), and Ainslie (2010). (Courtesy G. Potty).

where f is the acoustic frequency in kilohertz. The ordering of the terms in this equation is significant, as going from left to right the terms apply to progressively higher acoustic frequency. The first term, which is perhaps the least understood of the four, is related to boundary losses due to leakage out off the deep sound channel. The second term, which dominates at frequencies between a few hundred and a few thousand Hz, is due to borate ($B(OH)_3$) relaxation, which has a distinct pH dependence denoted by the coefficient A. Not much is known about the detailed geographical or seasonal variation of A (Lovett, 1980) but values for the Pacific (lower pH) and Atlantic (higher pH) Oceans are generally taken to be $A = 0.055$ and $A = 0.11$ respectively. The next term, which dominates from tens to hundreds of kHz, is associated with chemical relaxations due to magnesium sulfate ($MgSO_4$), and the last term is due to the viscosity of seawater.

When sound interacts with the seabed, acoustic loss can go up markedly. The fields of geo- and seismo-acoustics, which treat these complex seabed interactions, are, much like the present monograph, concerned with wave propagation through

a heterogeneous and stochastic medium. Rather than getting into these subjects, the idea here is to simply provide bulk properties of the seabed so as to enable shallow-water calculations of sound transmission through the stochastic internal-wave field. Typical geoacoustic parameters are summarized in Table 2.1.

2.4 Rays

Because of its strong geometric basis, ray theory applied to ocean acoustic propagation provides an extremely useful tool to understand the physics of sound scattering in the ocean (Flatté et al., 1979; Brown et al., 2003). In addition, ray theory provides the conceptual picture that is the foundation of many other approaches to sound scattering such as Born and Rytov theory, and Feynman path integrals. Here an overview of ray theory is presented that is meant to be brief but self contained. The emphasis will be on the Hamiltonian structure of the ray equations, and the topic of ray chaos will be introduced. Example calculations for a range-independent sound-speed profile, $c(z)$, will be presented and a qualitative discussion of internal-wave effects will be given.

2.4.1 Physical Picture and Basic Equations

There are a few ways to conceptualize and thus derive ray theoretical results. There is the variational approach that considers the ray to be an extremum of the travel time (Landau and Lifshitz, 1975; Gutzwiller, 1990), a methodology that is based on Fermat's principle (see Section 2.7.1). There is also the method of high-frequency asymptotic analysis of the wave equation (Frisk, 1994; Jensen et al., 1994), which has a pleasing rigor (see Section 2.4.2). Both of these methods will be presented in this chapter, but in this section a third method is put forward that is highly geometric in nature. Here the wave field of interest is considered to behave *locally* like a plane wave (Lighthill, 1978; Munk et al., 1995). Writing the local phase function as $\Theta(\mathbf{r}, t)$ then the plane wave approximation dictates that the vector wavenumber and scalar frequency are given by

$$\mathbf{k} = \boldsymbol{\nabla}\Theta, \tag{2.35}$$

$$\omega = -\frac{\partial \Theta}{\partial t}, \tag{2.36}$$

where ω and $\mathbf{k}$ are related by the plane wave dispersion relation, that is $\omega = \omega(\mathbf{k}, \mathbf{r})$. Taking the divergence of Eq. 2.36 and using Eq. 2.35, the following equation is obtained

$$\frac{\partial \mathbf{k}}{\partial t} = -\left(\frac{\partial w}{\partial \mathbf{k}} \cdot \boldsymbol{\nabla}\right)\mathbf{k} - \frac{\partial \omega}{\partial \mathbf{r}}. \tag{2.37}$$

Identifying $\mathbf{c_g} = \partial w/\partial \mathbf{k}$ as the group velocity and the total derivative in the direction of the wave as $d/dt = \partial/\partial t + \mathbf{c_g} \cdot \nabla$ then from Eq. 2.37 it follows quite naturally that the wave energy will follow along ray paths given by the Hamiltonian-like equations (Lighthill, 1978)

$$\frac{d\mathbf{r}}{dt} = \frac{\partial \omega}{\partial \mathbf{k}} = \mathbf{c_g}, \tag{2.38}$$

$$\frac{d\mathbf{k}}{dt} = -\frac{\partial \omega}{\partial \mathbf{r}}. \tag{2.39}$$

Here the dispersion relation plays the role of the Hamiltonian function. Equation 2.38 simply states that wave energy moves along the ray at the group velocity, and Eq. 2.39 states that the direction of propagation will change due to spatial variations in the dispersion relation (refraction). Here six equations are given to solve for the six unknowns, that is, three components each of the ray position and the wave vector. Lastly, as a consequence of the Hamiltonian structure of these equations it is seen that ω is constant along the rays (e.g., $d\omega/dt = 0$). These equations are quite general and can be applied to any wave system. A few examples include light, seismic waves, surface gravity waves, internal waves, and Rossby waves.

At this point it is useful to tailor the discussion to the problem of ocean acoustic propagation, where the dispersion relation for an ocean otherwise at rest is given by

$$\omega(\mathbf{r}, \mathbf{k}) = (k_x^2 + k_y^2 + k_z^2)^{1/2} c(\mathbf{r}). \tag{2.40}$$

For most ocean acoustic problems, only one-way wave propagation in a range-depth slice (x, z) need be considered. For propagation between fixed locations (e.g., sources and receivers), the convention is to use the range coordinate instead of the time coordinate as the independent variable. With these modifications the ray equations become

$$\frac{1}{\omega}\frac{dk_z}{dx} = -\frac{1}{(c^{-2} - k_z^2/\omega^2)^{1/2}}\frac{1}{c^3}\frac{\partial c}{\partial z}, \tag{2.41}$$

$$\frac{dz}{dx} = \frac{k_z}{\omega}\frac{1}{(c^{-2} - k_z^2/\omega^2)^{1/2}} = \tan\theta, \tag{2.42}$$

$$\frac{dT}{dx} = \frac{1}{c^2(c^{-2} - k_z^2/\omega^2)^{1/2}}, \tag{2.43}$$

where T is the acoustic travel time of the ray. It is evident that these equations are independent of acoustic frequency since $k_z \propto \omega$. Thus it is useful to define a frequency independent quantity $p_z = k_z/\omega = \sin\theta/c$ called the vertical ray slowness. Equations 2.41 and 2.42 with conjugate or phase space variables (z, p_z) are of

Hamiltonian form such that

$$\frac{dz}{dx} = \frac{\partial H}{\partial p_z}, \qquad \frac{dp_z}{dx} = -\frac{\partial H}{\partial z}, \tag{2.44}$$

where the convention is to define $H = -k_x/\omega = -(c^{-2} - p_z^2)^{1/2} = -\cos\theta/c$. The third equation is given by

$$\frac{dT}{dx} = L = p_z\frac{dz}{dx} - H = \frac{1}{c^2(c^{-2} - p_z^2)^{1/2}} = \frac{\sec\theta}{c}, \tag{2.45}$$

where L is the Lagrangian function. Equation 2.45 simply says that the ray moves along the ray path at the local sound speed, that is, $dT/ds = 1/c$ where $ds = (dx^2 + dz^2)^{1/2}$ is an infinitesimal ray arc length. In the parlance of Lagrangian dynamics and the variational approach to ray propagation (Fermat's principle), it is understood that the travel time of the ray path (e.g., the path integral of the Lagrangian function) is an extremum. These equations also indicate that the acoustic energy moving in the direction of the ray is perpendicular to the wave front (defined as a surface of constant phase). For a moving medium this is not the case (see Pierce, 1994; Munk et al., 1995; Ostashev and Wilson, 2015), but this situation will not be treated until Chapter 5.

In summary, these equations constitute a nonautonomous Hamiltonian system with one degree of freedom (Brown et al., 2003); z and p_z are canonically conjugate position and momentum variables, x is the independent variable, H is the Hamiltonian, L is the Lagrangian, and the travel time T corresponds to the action (kinetic energy minus potential energy) for a classical mechanics system. The system is nonautonomous because for the case of propagation through internal waves H will depend explicitly on the independent variable x. Ocean acoustics, as a Hamiltonian system, provides a unique view into the dynamics since the variational quantity that dictates the physics (e.g., travel time) is actually an observable quantity. This can be compared to the classical mechanics case where the action is not a direct observable (more later in Chapters 5 and 7).

The equations here are for the one-way Helmholtz equation but other Hamiltonian functions can be written down for approximations to the Helmholtz equation such as the parabolic approximation (Tappert and Brown, 1996; Brown et al., 2003). In the parabolic approximation a useful ray Hamiltonian function is given by

$$H = \frac{c_0 p_z^2}{2} + \frac{V(\mathbf{r})}{c_0}, \tag{2.46}$$

where $p_z = \tan\theta/c_0$ and the function $V = (1 - c_0^2/c^2)/2$ where c_0 is a reference sound speed. Here the ray equations take the particularly simple form

$$\frac{dp_z}{dx} = -\frac{1}{c_0}\frac{\partial V}{\partial z}, \tag{2.47}$$

$$\frac{dz}{dx} = c_0 p_z, \tag{2.48}$$

$$\frac{dT}{dx} = \frac{1}{c_0}\left(1 + \frac{c_0^2 p_z^2}{2} - V\right). \tag{2.49}$$

Note that in the PE travel time equation an extra factor of $1/c_0$ has been included on the right-hand side and this term comes from the $e^{iq_0 x}$ term in the PE equation (Simmen et al., 1997). Also related to the travel time equation it is found that $dT/ds \neq 1/c$, that is, the ray does not travel at the local sound speed. This is an artifact of the small-angle approximation. It is also recognized that the reference sound speed c_0 scales out of of Eqs. 2.47 and 2.48, so often the definition $p_z = \tan\theta$ is used. In this case the Hamiltonian has the dimensionless form $H = p_z^2/2 + V$, and the Lagrangian function is $L = p_z^2/2 - V$, which yields a variational principle in which the ray is an extremum of the acoustic path length S_a or distance along the ray. This oddity is a result of introducing the scaling parameter c_0 into the parabolic equation so that time and length are interchangeable, that is, the ray travel time is related to the path length by $T = S_a/c_0$.

The ray equations as discussed so far (Eqs. 2.44 and 2.45) allow calculation of the wave phase as a function of position and time, that is the acoustic pressure field is given by

$$p(\mathbf{r}, t) = \sum_j a_j(\mathbf{r}, t) e^{i\omega(T_j(\mathbf{r}) - t)}, \tag{2.50}$$

where the sum is over all rays that pass through the position $\mathbf{r}$. The only remaining piece of information that is needed to predict the pressure field is the ray amplitude a_j, which is discussed next.

2.4.2 Ray Theory: Asymptotic Analysis

While quite standard in many ocean acoustics textbooks (Jensen et al., 1994; Pierce, 1994), the asymptotic analysis that leads to the ray equations will be presented here so that the reader may see the geometric derivation discussed in the previous section in a different light. Here the ray amplitude equation will be derived for use in subsequent chapters. The starting point is the Helmholtz equation, where the Anzatz $p(\mathbf{r}, \omega) = a(\mathbf{r}, \omega)\exp(i\Theta(\mathbf{r}, \omega))$ is used. Plugging this expression into the Helmholtz equation yields equations for the real and imaginary

parts that are given by

$$\nabla^2 a - a|\nabla\Theta|^2 + \frac{\omega^2}{c^2}a = 0, \tag{2.51}$$

$$2\nabla\Theta\cdot\nabla a + a\nabla^2\Theta = 0. \tag{2.52}$$

In the high-frequency limit one expects $\Theta \propto \omega$ and thus in Eq. 2.51 the last two terms are proportional to ω^2 while the first term has no frequency dependence. This yields the *Eikonal* equation written

$$|\nabla\Theta|^2 = \frac{\omega^2}{c^2}. \tag{2.53}$$

This equation defines the geometry of the ray paths which are lines perpendicular to the wave fronts for which Θ is a constant. The equation can also be interpreted in terms of Eqs. 2.35 and 2.36, thus giving the plane wave dispersion relation. Standard techniques, which will not be repeated here, can be used to render the Eikonal equation into a form suitable for computing ray trajectories (Jensen et al., 1994; Pierce, 1994) giving

$$\frac{d}{ds}\left(\frac{1}{c}\frac{d\mathbf{r}}{ds}\right) = -\frac{1}{c^2}\nabla c. \tag{2.54}$$

With some manipulation this second-order differential equation can be shown to be equivalent to the first-order Hamiltonian equations presented in the previous section.[3]

The ray amplitude equation can be interpreted geometrically. A unit vector in the direction of the ray can be written as $\mathbf{k}/q_0 = \nabla\Theta/q_0$, so the first term in Eq. 2.52 has the form $2q_0 da/ds$ where da/ds is the rate of change of the ray amplitude in the direction of or along the ray. So, the ray amplitude equation has the form

$$2q_0\frac{da}{ds} + a\nabla\cdot\mathbf{k} = 0, \tag{2.55}$$

which says that the rate of change of the ray amplitude is proportional to the divergence of the rays.[4] This interpretation follows the intuition that a diverging/converging bundle of rays will have decreasing/increasing amplitude. More about this matter follows in the next section.

2.4.3 Ray Amplitude and Stability

Ray theory gives us a means to understand the variation of acoustic amplitude through the ocean, and this issue is critically connected to the subject of ray path

[3] Also see the variational approach to ray propagation presented in Section 2.7.

[4] The factor of two q_0 in the first term comes from the fact that the ray amplitude is being solved for. In the next section where energy considerations are addressed (e.g., quadratic quantities) a simpler result follows.

stability. In the absence of any dissipation, it is well known that wave energy is conserved along ray bundles (Lighthill, 1978; Pierce, 1994; Brown et al., 2003). For wave energy density W and power flux $\mathbf{I} = W\mathbf{c_g}$ the energy conservation equation is written

$$\frac{\partial W}{\partial t} + \boldsymbol{\nabla} \cdot \mathbf{I} = 0. \tag{2.56}$$

Expanding the divergence, this equation can be cast as a total time derivative along the ray giving $dW/dt = -W\boldsymbol{\nabla} \cdot \mathbf{c_g}$. Hence the change in the local wave energy density is proportional to minus the divergence of the group velocity of a ray bundle, that is, the intuitive result is obtained that a diverging bundle has decreasing energy density while a converging bundle has increasing energy density. Equation 2.56, however, is not useful for computing ray amplitudes because evaluation of $\boldsymbol{\nabla} \cdot \mathbf{c_g}$ requires knowledge of nearby ray trajectories. Instead an equation is sought that can be integrated together with the ray trajectory and travel time equations (Eqs. 2.44 and 2.45). This can be achieved by carrying out a traditional stability analysis of the ray equations (Tabor, 1989).

Consider the stability of a ray with respect to variations in the initial conditions. Using the chain rule, the resulting changes in the variables p_z and z are thus written

$$\delta p_z = \left.\frac{\partial p_z}{\partial p_0}\right|_{z=z_0} \delta p_0 + \left.\frac{\partial p_z}{\partial z_0}\right|_{p_z=p_0} \delta z_0, \qquad \delta z = \left.\frac{\partial z}{\partial p_0}\right|_{z=z_0} \delta p_0 + \left.\frac{\partial z}{\partial z_0}\right|_{p_z=p_0} \delta z_0, \tag{2.57}$$

where $(\delta p_0, \delta z_0)$ are the perturbations to the initial condition (p_0, z_0), and $(\delta p_z, \delta z)$ are the resultant perturbations to the ray. Writing this in matrix form, the result is

$$\begin{pmatrix} \delta p_z \\ \delta z \end{pmatrix} = \mathbf{Q} \begin{pmatrix} \delta p_0 \\ \delta z_0 \end{pmatrix}, \tag{2.58}$$

where the stability matrix $\mathbf{Q}$ is given by

$$\mathbf{Q} = \begin{pmatrix} q_{11} & q_{12} \\ q_{21} & q_{22} \end{pmatrix} = \begin{pmatrix} \left.\frac{\partial p_z}{\partial p_0}\right|_{z_0} & \left.\frac{\partial p_z}{\partial z_0}\right|_{p_0} \\ \left.\frac{\partial z}{\partial p_0}\right|_{z_0} & \left.\frac{\partial z}{\partial z_0}\right|_{p_0} \end{pmatrix}. \tag{2.59}$$

Now the question is how do the elements in the stability matrix evolve in range. As an example it is helpful to examine one of the elements, $\partial z/\partial p_0$. Taking the range derivative the result is

$$\frac{d}{dx}\frac{\partial z}{\partial p_0} = \frac{\partial}{\partial p_0}\frac{dz}{dx} = \frac{\partial^2 H}{\partial p_z^2}\frac{\partial p_z}{\partial p_0} + \frac{\partial^2 H}{\partial z \partial p_z}\frac{\partial z}{\partial p_0}, \tag{2.60}$$

where Hamilton's equations have been used. Considering all the elements in this way the stability equations become

$$\frac{d}{dx}\mathbf{Q} = \mathbf{K}\mathbf{Q}, \qquad \mathbf{K} = \begin{pmatrix} -\frac{\partial^2 H}{\partial z \partial p_z} & -\frac{\partial^2 H}{\partial z^2} \\ \frac{\partial^2 H}{\partial p_z^2} & \frac{\partial^2 H}{\partial z \partial p_z} \end{pmatrix}, \tag{2.61}$$

where $\mathbf{K}$ is termed the propagator matrix and the initial condition for $\mathbf{Q}$ is the identity matrix. Physically the stability matrix tells us the variation in (z, p_z) at range x with respect to initial variations in the source depth and angle. For the case of a point source the variation of the source depth is irrelevant, and the critical term in the stability matrix is q_{21}, that is, the variation in the depth of the ray with respect to an initial variation in vertical ray slowness (i.e., variation in initial angle). There are also stability equations for travel time, which are given here for completeness and future use

$$\frac{d}{dx}\left(\left.\frac{\partial T}{\partial p_0}\right|_{z_0}, \left.\frac{\partial T}{\partial z_0}\right|_{p_0} \right) = p_z \left(\frac{\partial^2 H}{\partial p_z^2}, \frac{\partial^2 H}{\partial z \partial p_z} \right) \mathbf{Q}. \tag{2.62}$$

A simple geometric calculation for the ray amplitude at position (x,z) gives (Brown, 1994; Tappert and Tang, 1996)

$$a(x,z) = a_0 \frac{r_0}{\sqrt{x}} \frac{\mathrm{e}^{-iM\pi/2}}{\sqrt{|H(x,z)|\,|q_{21}(x,z)|}}, \tag{2.63}$$

where $r_0 = 1$ m is the standard reference range and a_0 is the reference amplitude. For $a_0 = 1$, the transmission loss (TL) given by $20\log_{10}|a|$ is obtained. The ray amplitude equation can be better understood by looking at the small range behavior (e.g., $x \to 0$). In this limit the result is $q_{21}(x) \simeq x(\partial^2 H(0)/\partial p^2) = x c_s / \cos^3\theta_0$, and $H(0) = -\cos\theta_0 / c_s$, where c_s and θ_0 are the sound speed and ray angle at the source. This yields $a(x,r) = a_0 r_0 \cos\theta_0 / x = r_0 / s$, where the slant range is $s = x/\cos\theta_0$. Thus the normalization yields spherical spreading at short range, and for $a_0 = 1$ the conventional TL of zero at the slant range of $r_0 = 1$ m is recovered.

The quantity M, termed the Maslov index, is the number of caustics that the ray has passed through. A ray has passed through a caustic when the stability matrix element q_{21} passes through zero, which means that two nearby rays have crossed one another. The crossing yields a π phase shift for q_{12}, and thus a $\pi/2$ phase shift in Eq. 2.63. Caustics are high-intensity regions of the wave field and are therefore of great interest. However, the troubling result is found that ray theory predicts an intensity singularity at caustics. There are methods to remove the singularities for the case in which the sound speed is only a function of depth or the range dependence is extremely weak (Brown, 1994), but these methods are not applicable to the problem of sound propagation through the stochastic

internal-wave field because of the abundance of caustics created by the internal waves. While ray theory has this shortcoming with regard to caustics, nonetheless the theory does have the advantage of indicating precisely where the caustic regions are located.

The stability equations in the parabolic approximation are of great interest, and these results will be used extensively in the development of fluctuation theory using the method of path integrals. With the PE Hamiltonian (Eq. 2.46), the propagator matrix K has a simple form and writing $q_{21} = \xi$ the result is

$$\frac{d^2\xi}{dx^2} + V''\xi = 0, \tag{2.64}$$

where $V'' = \partial^2 V/\partial z^2$ is the second derivative along the ray path. Using the terminology of Flatté et al. (1979), Eq. 2.64 is called the ray-tube equation and the function ξ is called the ray tube function.[5] Here it is seen that ξ, and thus the ray amplitude, depends critically on the curvature of the sound-speed profile. For deterministic cases this means that the sound-speed field must be known precisely to compute the ray amplitude, and this result shows that acoustic amplitudes are most sensitive to small vertical scale structure in the ocean.

With knowledge of the amplitude the ray theory description of the pressure field is complete. The acoustic pressure for a given range and receiver depth is then a coherent sum over all the rays connecting the source and receiver: These paths are termed eigenrays. Assuming propagation free of attenuation this coherent sum can be written

$$p(x,z,t) = \sum_{j=1}^{N} a_j(x,z)\, E(T_j - t)\, \mathrm{e}^{i\omega_c(T_j - t)}, \tag{2.65}$$

where T_j and a_j are the eigenray travel time and amplitude, N is the number of eigenrays, $E(T_j - t)$ is the unit amplitude pulse envelope, and ω_c is the carrier frequency. Depending on the signal bandwidth, which dictates the temporal width of the pulse envelope, the eigenrays may be interfering (e.g., overlapping in time) or they may form isolated arrivals.

2.4.4 Ray Chaos: Introduction

It has been well established that ray propagation through the stochastic internal-wave field results in exponential growth of the stability matrix elements (Beron-Vera et al., 2003; Brown et al., 2003). This exponential sensitivity to initial conditions is termed ray chaos, and it is central to the understanding of

[5] The ray-tube equation can also be derived directly from the PE ray equation, $d^2z/dx^2 + V' = 0$ (see Eqs. 2.47 and 2.48) by examining perturbations around a ray given by $z(x) = z_r(x) + \xi(x)$, where z_r is the ray trajectory. Plugging z into the ray equation and expanding around the ray path to first order in ξ, Eq. 2.64 is easily obtained.

ocean acoustic propagation. Ray chaos is also related to exponential sensitivity to perturbations in sound speed like those caused by internal waves. Of course it is not enough to simply say there is ray chaos; the growth rate of the instability must be estimated: this factor is called the Lyapunov exponent. The basic theory for the Lyapunov exponent is presented here and this subject is developed further in Chapter 5. There is a wealth of literature on dynamical systems stability and the interested reader is referred to the textbook by Tabor (1989) and the review article by Brown et al. (2003), which cover well the fundamentals. What follows is a brief self-contained overview.

The ray equations for an initial launch angle and depth will be stable or nonchaotic if there is a constant Υ along the ray trajectory such that

$$\frac{d\Upsilon}{dx} = \frac{\partial \Upsilon}{\partial z}\frac{dz}{dx} + \frac{\partial \Upsilon}{\partial p}\frac{dp}{dx} + \frac{\partial \Upsilon}{\partial x} = 0. \tag{2.66}$$

For $c = c(z)$, then $\Upsilon = H = -\cos(\theta)/c$ is a ray constant (i.e., the horizontal wavenumber) and all rays are stable or integrable; that is the equations of motion can be written in terms of an explicit integral or quadrature.[6] For ocean sound-speed structure that is generally a complicated function of both depth and range, like that caused by stochastic internal waves, there are no obvious ray constants, and extensive calculations show no indications of stable trajectories (Beron-Vera et al., 2003; Brown et al., 2003). Thus with a high degree of certainty all ray trajectories are assumed to be unstable. In this case the growth rate of the instability or the Lyapunov exponent is a critical piece of information. Furthermore, since there is a stochastic medium in the ocean, the Lyapunov exponent itself will be a stochastic variable whose moments and distribution function will be of critical interest.

An analysis of the stability matrix $\mathbf{Q}$ gives the key information. First, $\mathbf{Q}$ has some important properties. For Hamiltonian systems it can be shown that phase space "flow" $(dz/dx, dp_z/dx)$ satisfies the incompressibility condition,

$$\frac{\partial}{\partial z}\frac{dz}{dx} + \frac{\partial}{\partial p_z}\frac{dp_z}{dx} = 0, \tag{2.67}$$

and thus phase space volume is conserved regardless of the form of the Hamiltonian (Tabor, 1989). This is Liouville's theorem. So, $\mathbf{Q}$ can be viewed as a linear, canonical transformation and as such its determinant is unity. At finite range, x, the stability of a ray path is determined from the eigenvalues of $\mathbf{Q}$. It is well known that $\mathbf{Q}$ can be diagonalized by a linear, similarity transformation

$$\Lambda = \mathbf{L}\mathbf{Q}\mathbf{L}^{-1} \Rightarrow \begin{pmatrix} \lambda_1 = \lambda & 0 \\ 0 & \lambda_2 = \lambda^{-1} \end{pmatrix}. \tag{2.68}$$

[6] The constancy of $\cos(\theta)/c$ is termed Snell's law.

The last form applies to systems with a single degree of freedom because the determinant is unity. The similarity transformation is known to leave Tr(**Q**) invariant, and it is found that Tr(**Q**) is real. A well known result is (Tabor, 1989; Brown et al., 2003)

$$\text{For } |\text{Tr}(\mathbf{Q})| > 2, \lambda_1 \simeq \text{Tr}(\mathbf{Q}), \lambda_2 = 1/\lambda_1 \simeq 0, \text{Unstable Motion}, \tag{2.69}$$

$$\text{For } |\text{Tr}(\mathbf{Q})| < 2, \qquad \lambda_{1,2} = \exp(\pm i\alpha), \qquad \text{Stable Motion}. \tag{2.70}$$

Traditionally under strong instability one writes

$$|\text{Tr}(\mathbf{Q})| \simeq \lambda_1 \equiv \exp(\nu x), \tag{2.71}$$

which is the definition of the finite-range Lyapunov exponent, ν, describing the local exponential divergence of nearby ray trajectories. Under stable conditions, namely when the sound speed is only a function of depth, nearby ray trajectories diverge in range by and large linearly. The largest Lyapunov exponent is expressed as

$$\nu_L = \lim_{x\to\infty} \frac{\ln(|\text{Tr}(\mathbf{Q})|)}{x}, \tag{2.72}$$

and in this limit all values of ν approach ν_L. The rays with nonzero Lyapunov exponent are termed chaotic rays because of their exponential sensitivity to initial conditions.

An interesting consequence of the exponential divergence of nearby ray trajectories is that the intensities of chaotic rays, which are proportional to $|\partial z/\partial p_0|^{-1}$, decay exponentially with range and therefore would be difficult to detect in experiments. On the other hand, energy conservation considerations suggest and numerical experiments show (Tappert and Tang, 1996) that under chaotic conditions the number of eigenrays increases exponentially with range and therefore collectively chaotic rays may be detectable in experiments.

This is where the subject will stand for now. The issue of ray stability will be further investigated in Chapter 5.

2.4.5 Ehrenfest Theorem

The significance of the ray picture is demonstrated by the important result of Ehrenfest (1927), who showed that the mean position and momentum of a quantum wavepacket follows the classical trajectory (see Merzbacher (1961) or Sakurai (1985)). In this section it will be shown that for acoustic propagation in the parabolic approximation the mean position and angle of propagation of the wavepacket in the vertical will follow the ray equations. This topic is relevant

to the problem of sound propagation through the stochastic internal-wave field since chaotic ray dynamics are known to invalidate the correspondence between full wave– and ray-based representations after the waves have propagated over a distance termed the Ehrenfest range (Brown et al., 2003). For classical/quantum systems this breakdown is called the Ehrenfest time (Zaslavsky, 1980).

The mean vertical position of the wavefunction is defined as

$$\langle z\rangle = \int A^*(z,x)\, z\, A(z,x)\, dz. \tag{2.73}$$

Taking the x-derivative and using the parabolic equation the result is

$$\begin{aligned}\frac{d}{dx}\langle z\rangle &= \int\left[\frac{\partial A^*(z,x)}{\partial x} zA(z,x) + A^*(z,x) z \frac{\partial A(z,x)}{\partial x}\right] dz,\\ &= \frac{i}{2q_0}\int\left[A^* z\frac{\partial^2 A}{\partial z^2} - \frac{\partial^2 A^*}{\partial z^2} zA\right] dz.\end{aligned} \tag{2.74}$$

The integrand of Eq. 2.74 has the form

$$\frac{\partial}{\partial z}\left[A^* z\frac{\partial A}{\partial z} + A^*A - \frac{\partial A^*}{\partial z} zA\right] - 2A^*\frac{\partial A}{\partial z}. \tag{2.75}$$

Integrating Eq. 2.74, the first term is seen to be a total derivative, so it can be evaluated at the boundaries where A must be zero in order to have finite energy. Thus the result for the range evolution of the mean vertical position is

$$\frac{d}{dx}\langle z\rangle = \int A^*\left(\frac{-i}{q_0}\frac{\partial}{\partial z}\right) A\, dz. \tag{2.76}$$

Next it should be noted that the operator $p = (-i/q_0)\partial/\partial z$ appears in the parabolic equation such that

$$\frac{i}{q_0}\frac{\partial A}{\partial x} = \left(\frac{p^2}{2} + V(x,z)\right)A \equiv H_{op}(p,z,x)A,$$

where the Hamiltonian operator H_{op} has the same form as the ray Hamiltonian (Eq. 2.46). One may also view the momentum operator p as generating vertical translations, so that $pA \simeq k_z A/q_0 = A\tan\theta$; hence p is related to c_0 times the ray slowness p_z. Thus from Eq. 2.76 the final result is that the average depth position follows the ray trajectory equation (Eq. 2.48), that is,

$$\frac{d}{dx}\langle z\rangle = \langle p\rangle. \tag{2.77}$$

A similar (but tedious) calculation can be done for the range evolution of the canonical variable p, related to the wave angle. Here it is found that

$$\frac{d}{dx}\langle p\rangle = \int\left[\frac{\partial A^*(z,x)}{\partial x}pA(z,x) + A^*(z,x)p\frac{\partial A(z,x)}{\partial x}\right]dz,$$
$$= \int -A^*\frac{\partial V}{\partial z}A\, dz = -\left\langle\frac{\partial V}{\partial z}\right\rangle, \tag{2.78}$$

which is nearly the full wave equivalent of the ray equation Eq. 2.47. The only thing that limits us from making a perfect ray-to-wave analogy is that

$$\left\langle\frac{dV}{dz}\right\rangle \neq \frac{d}{d\langle z\rangle}V(\langle z\rangle). \tag{2.79}$$

For equality in Eq. 2.79 to hold then $V(z)$ must be a slowly varying function of z, relative to the vertical spread of the wave functions A. Physically this means that diffraction is weak.

2.4.6 Rays in a Range-Independent Ocean

In this section various ray-derived quantities are discussed for the case in which the sound speed is only a function of depth. Useful example calculations are provided to give important insight into ocean acoustic propagation, and they provide a benchmark from which to compare calculations involving internal-wave sound-speed perturbations. For simplicity and ease of reproduction by the reader, results are shown for the mid-latitude Munk canonical profile (Eq. 2.28) where parameters of $B = z_a = 1000$ m, and $c_A = 1500$ m/s are chosen. For this example a point source at the sound channel axis is considered and all the rays are nonsurface interacting. Examples for shallow-water propagation are not presented since the mode approach proves much more useful for that case. Properties of ray quantities in a range-independent profile have been discussed in many textbooks (e.g., see Munk et al., 1995), so only a brief account is given here.

Ray Paths

Figure 2.4 shows a collection of ray paths for the Munk sound-speed profile. In this case the Hamiltonian function is conserved (i.e., horizontal wavenumber is constant) meaning that $\cos\theta/c$ is a constant along a ray (i.e., Snell's law). Thus it is useful to define a quantity for identifying particular ray paths called the grazing angle, which is the absolute value of the ray angle at the sound-channel axis, namely $\cos(\theta_g) = c_{axis}/c_{turn}$ where c_{axis}/c_{turn} are the sound speed at the axis/ray turning point. A turning point is where the ray angle is zero, and the upper and lower turning point depths are labeled z^+ and z^- respectively. High grazing angle

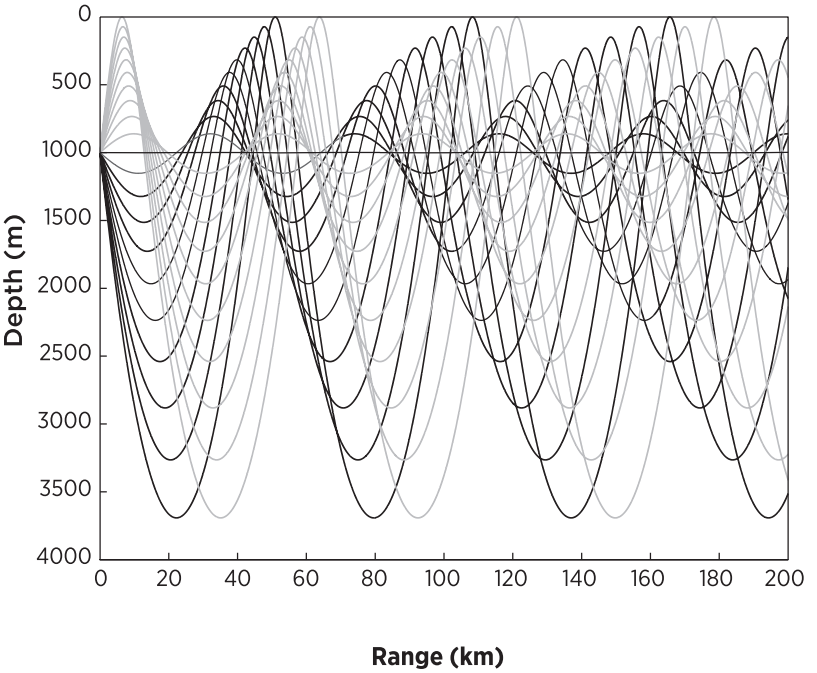

Figure 2.4. A selection of rays computed for the Munk canonical profile (Eq. 2.28). Initially upward/downward rays are colored gray/black.

rays have turning points quite distant from the sound-channel axis, while low grazing angle rays are confined vertically near the axis. In this particular case the grazing angles are between 0° and 12.6°.

For a range-independent Munk profile, rays of a given grazing angle are periodic in range but asymmetrical above and below the axis. For this mid-latitude profile, the rays have a short upper loop that extends above the axis and a longer lower loop below the axis. The combination of the upper and lower loop is termed the ray double loop. For small grazing angles the upper and lower loops become symmetrical and the double loop appears more sinusoidal. Furthermore, as the grazing angle increases so does the horizontal double loop distance. The upper/lower horizontal loop distances $R^{\pm}$, and the travel time to traverse a loop $T^{\pm}$ can be easily derived from the ray equations with the result

$$R^{\pm} = 2\int_{z_a}^{z^{\pm}} \frac{c^{-1}(z^{\pm})}{\sqrt{c^{-2}(z) - c^{-2}(z^{\pm})}}\, dz, \tag{2.80}$$

$$T^{\pm} = 2\int_{z_a}^{z^{\pm}} \frac{c^{-2}(z)}{\sqrt{c^{-2}(z) - c^{-2}(z^{\pm})}}\, dz. \tag{2.81}$$

The double loop distance and time are $R_L = R^+ + R^-$ and $T_L = T^+ + T^-$. The ray double loop distance is important to scattering because of a ray loop resonance condition (Cornuelle and Howe, 1987; Munk et al., 1995) that makes rays most sensitive to ocean structure on the scale of R_L and its harmonics (more in Chapters 4 and 5). Another important quantity is the horizontal loop group velocity of a ray, defined as $c_g^{\pm} = R^{\pm}/T^{\pm}$. This quantity also varies as a function of grazing angle and upper/lower loop. At low grazing angles both the upper and lower loops have horizontal group speeds close to the axial sound speed, but as grazing angle increases, upper loops slow down while lower loops speed up. The horizontal double loop group speed R_L/T_L, however, increases with grazing angle, that is, the lower loop dominates. The properties that have been discussed for the mid-latitude/Munk profile also can help understand the polar and shallow-water cases because polar rays act like lower loops, and shallow-water cases act like upper loops. This dispersive behavior of the loops as a function of grazing angle has important consequences for the geometries of the wave front and time front which are discussed next.

Time Front

An important observational ray quantity is the time front, which is ray depth versus travel time for a fixed range (see Figure 2.5). This display shows how the wave front sweeps by a set of vertical receivers at fixed range. The accordion pattern seen in the display is formed by the folding of the wave front by the sound channel (loop dispersion), and the differences in wave speed from initially up-going (upper loop first) and down-going (lower loop first) rays. As previously discussed for the Munk profile, and general deep-water profiles, low grazing angle rays move down range more slowly than high grazing angle rays, so the time front is seen to spread out in depth from late to early arrival times.[7] The time front is seen to be composed of branches that terminate in depth with a cusp shape. The cusped regions are termed caustics where singularities exist. The branches are made up of rays with similar properties, namely all rays on a branch have the same number of ray turning points. Thus each branch can be labeled with a unique identifier (ID), which is the number of ray turning points and a plus/minus sign depending on whether the rays have an initial up/down angle at the source (up means the ray is pointing towards the ocean surface). Because early arriving branches are composed of high grazing angle rays with long double loop lengths they have fewer turning points (and thus a smaller ID number) compared to the low grazing angle branches. As range increases/decreases loop dispersion dictates that there will be more/fewer branches in the time front.

[7] For a polar profile the time front has this same pattern because in both cases the loop dispersion is dominated by the lower loops. In shallow water the low grazing angles are faster and thus the time front widens in depth from early to late travel times.

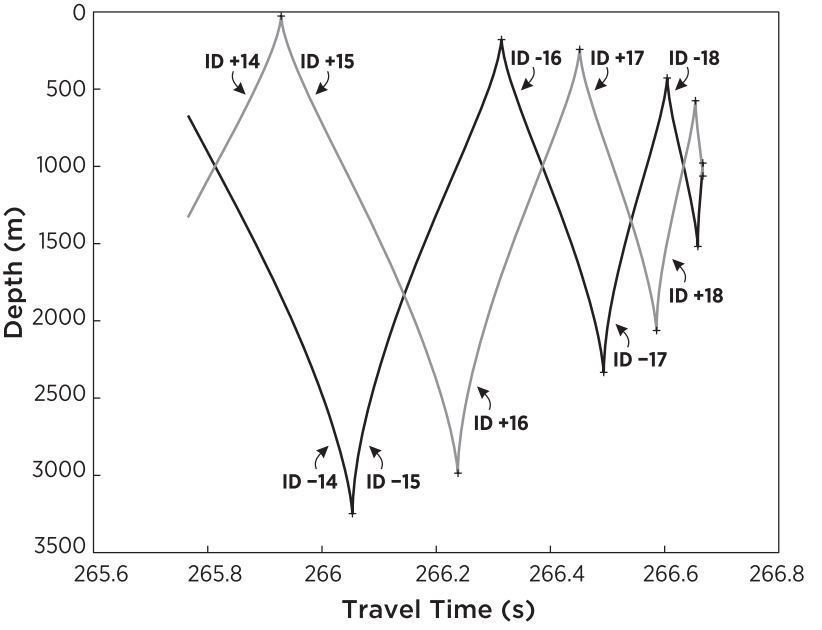

Figure 2.5. Time front for the Munk canonical profile for a range of 400 km. Initially upward/downward rays are colored gray/black. Caustics are marked with black crosses, and time front IDs are labeled.

Much of the progress that has been made in the subject of sound transmission through the stochastic internal-wave field is due to the ability to observe the evolution of time fronts over a large vertical aperture. When internal waves are included in the ray calculation, it has been discovered that the basic time front pattern for the early arrivals is not dramatically altered, although the caustic cusps are observed to vertically elongate, spreading into the shadow zones. These rays scatter primarily along the time front as opposed to across it due to small-angle scattering effects. For the late arrivals the ray scattering is strong enough to destroy the branch pattern, and significant vertical spreading of acoustic energy into the shadow zone is observed (more in Chapter 5).

Eigenray Plot: Caustics

Further information regarding the acoustic field is provided by an eigenray plot, which is a display of ray depth at the final range versus initial ray angle (see Figure 2.6). Eigenrays are identified in this plot by drawing a horizontal line at the receiver depth and noting the launch angles at which the eigenray curve intersects the receiver depth. The slope of this curve $\partial z/\partial\theta_0$ is proportional to the stability matrix quantity $q_{12} = \partial z/\partial p_0$ and thus gives us information about caustics and the ray amplitude. Caustics occur where the slope is zero.

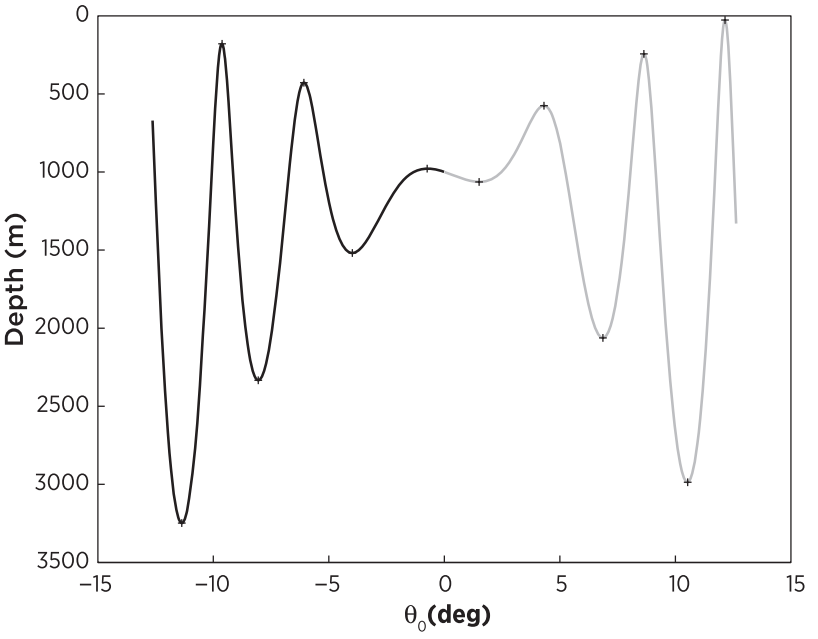

Figure 2.6. Eigenray plot showing ray depth versus initial angle for the Munk canonical profile at a range of 400 km. Caustics occur where the slope of the curve passes through zero (i.e., $\partial z/\partial\theta_0 = \partial z/\partial p_0 = 0$) , and these points are marked with black crosses.

When internal waves are added to the ray calculation, the eigenray plot can develop complex structure because ray chaos leads to an exponential growth of eigenrays and therefore of caustics. Theoretical approaches such as weak fluctuation theory and path integrals that expand about the unperturbed ray assume that the eigenrays created by the internal-wave fluctuations remain close to the unperturbed ray. This is not always a good assumption (more in Chapter 5).

Lagrangian Manifold

Yet another way of interpreting the ray acoustic field is to plot the Lagrangian manifold, that is a depth versus momentum display (Figure 2.7). At the initial range the manifold is a horizontal line at the source depth. As the rays propagate out in range, each point on the manifold (representing different rays with different launch angles) start rotating in a closed loop; the loop is closed because the rays are periodic with double loop length R_L. Because low grazing angle rays have shorter double loop lengths than high grazing angle rays, the center of the manifold rotates more rapidly as the rays propagate out in range. This loop dispersion (i.e., grazing angle dependence of loop length) then creates the swirling pattern of the manifold. The Lagrangian manifold can become folded and stretched but it cannot break owing to phase space area preservation (Liouville's theorem). Note that in

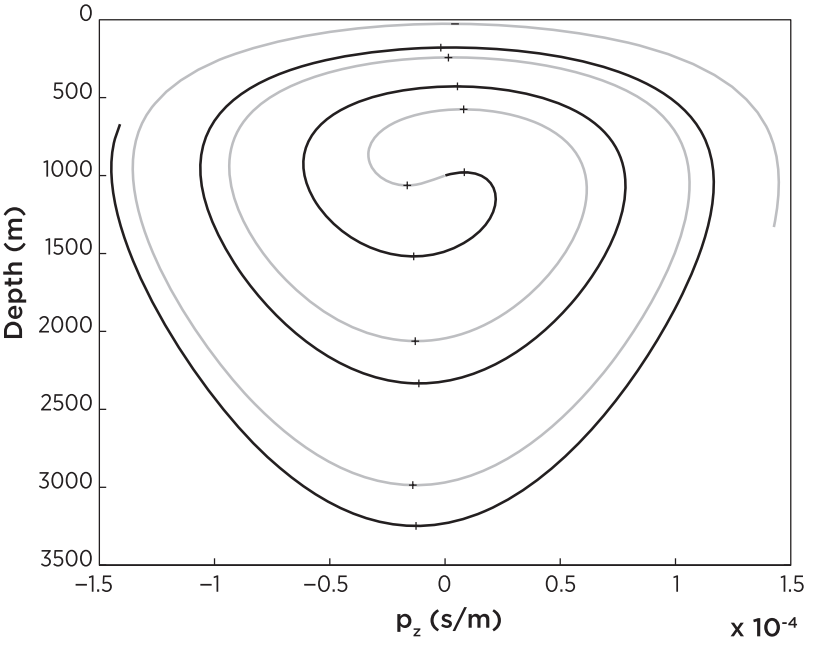

Figure 2.7. Lagrangian manifold for the rays in Munk canonical profile at a range of 400 km. Initially upward/downward rays are colored gray/black. Caustics are marked with vertical black crosses.

the Lagrangian manifold display in Figure 2.7 caustics are not located at $p_z = 0$, and this means that the cusps are slightly tilted.

The range evolution of the Lagrangian manifold is closely related to an equivalent set of canonical variables termed action-angle variables (Brown et al., 2003). For the case in which $c = c(z)$, there exists a canonical transformation from (z, p_z) to (I, θ) that yields a Hamiltonian that depends on the action coordinate I, and not the angle coordinate θ. Thus Hamilton's equations become

$$\frac{d\theta}{dx} = \frac{\partial H}{\partial I} \equiv K_L(I), \quad \frac{dI}{dx} = -\frac{\partial H}{\partial \theta} = 0. \tag{2.82}$$

The solution to these equations is simply $I =$ constant and $\theta(x) = K_L(I)x + \theta(0)$. The factor $K_L(I)$ is equal to $2\pi/R_L(I)$ and gives us the rotation rate of the points along the Lagrangian manifold as the rays propagate out in range.[8] The action variable is written

$$I = \frac{1}{2\pi} \oint p(z)dz = \frac{1}{\pi} \int_{z^-}^{z^+} p(z)dz, \tag{2.83}$$

where the integration is over one cycle of the ray's periodic trajectory. Action angle variables will be discussed in more detail in Chapter 5.

[8] The notation here is a departure from the literature which uses ω instead of K_L.

When internal-wave sound-speed fluctuations are added to the problem, the Lagrangian manifold, like the eigneray plot, will develop complex structure. The rays are no longer periodic, and the action is not constant. In Chapter 5 it will be shown that the degree of complexity in the Lagangian manifold and other acoustic quantities will be strongly influenced by the factor dK_L/dI, where K_L is computed from the background sound-speed profile. Physically this factor tells us how strongly the background profile shears the manifold: Strongly sheared regions of the manifold are associated with the strongest acoustic variability. This sensitivity to the background sound-speed profile was one of the major discoveries of the last 30 years of ocean acoustics research.

Ray Intensity

Lastly the ray TL computed from the stability equations (see Figure 2.8) is shown. Here it is evident that the TL becomes exceedingly low at the caustics, a result of the divergence of the ray amplitude there. The focusing effect of the waveguide is also evident. Rays with small grazing angles are gathered together near the sound channel axis and experience smaller loss. Higher grazing angle rays are not as effectively focused by the waveguide and experience greater loss.

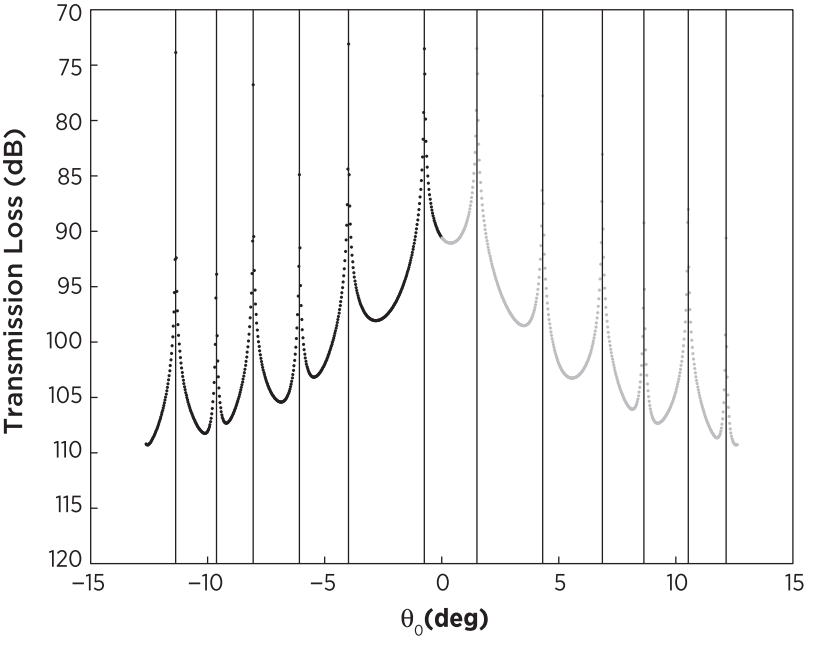

Figure 2.8. Transmission loss (TL) versus initial ray angle for the rays in the Munk canonical profile at a range of 400 km. Caustics are marked with vertical black lines.

2.5 Fresnel Zones and Ray Tubes

Ray theory tells us that sound travels along specific ray paths that connect the source and receiver, but this physical picture cannot be entirely true because it has been seen that when nearby ray paths get too close, singularities occur in the predicted wave field amplitude. Further progress with this problem can be made if one considers the possibility that nearby rays, not necessarily eigenrays, can interfere with one another. This idea will be investigated here using the notion of a Fresnel zone, that is, a region of interfering paths near a particular eigenray. These nearby paths can be physically associated with diffraction. It is important to stress that this treatment of Fresnel zones will not solve the problem of ray theory singularities, but it will allow us to think beyond the idea of a narrow ray, a concept that is critical in the Born and Rytov scattering theory (Section 2.6 and Chapter 6) as well as path integral theory (Section 2.7 and Chapter 7).

To start the analysis requires a way to quantify acoustic phase for an arbitrary path, and here ray theory is useful. At this point in the analysis it is best to examine the simple case in which the sound speed is only a function of depth. The effects of internal waves will be discussed at length in subsequent chapters. Accordingly the accumulated phase, $\Theta(\mathbf{x}_0, \mathbf{x}_R)$, along a ray path Γ starting at position $\mathbf{x}_0$ and ending at location $\mathbf{x}_R$ will be given by

$$\Theta(\mathbf{x}_0, \mathbf{x}_R) = \omega \int_\Gamma \frac{ds}{c} = q_0 \int_\Gamma \left[\frac{\dot{z}^2}{2} - V(z) \right] dx, \tag{2.84}$$

where the last line follows from the parabolic approximation (see Eq. 2.49), with $\dot{z} = dz/dx$ and $q_0 = \omega/c_0$. Here tradition is followed and the Fresnel zone calculation is carried out in the parabolic approximation (Flatté et al., 1979; Flatté, 1983). While this approximation is not absolutely necessary, it simplifies the treatment from a pedagogical standpoint and allows a greater appreciation of the literature. In fact, to the best of our knowledge no one has carried out the calculation without the parabolic approximation, though it would be simple to do so.

An equation is sought for the phase function in the vicinity of a geometric ray path, and the focus initially is on nearby paths that are separated vertically from the geometric path. This leads to the vertical Fresnel zone. The vertical Fresnel zone will be seen later to be important because of the ocean waveguide and the small-scale vertical structure of internal waves. For a point source the vertical separation of a nearby ray is given by the stability matrix element q_{21}. In the parabolic approximation, the ray-tube equation (Eq. 2.64) gives this separation.

To find the phase of ray paths near a particular ray $z_r(x)$, one writes $z = z_r(x) + \xi(x)$, where it is required that ξ goes to zero at the source and receiver, that is, the nearby path must connect the source and receiver. Plugging this expression into

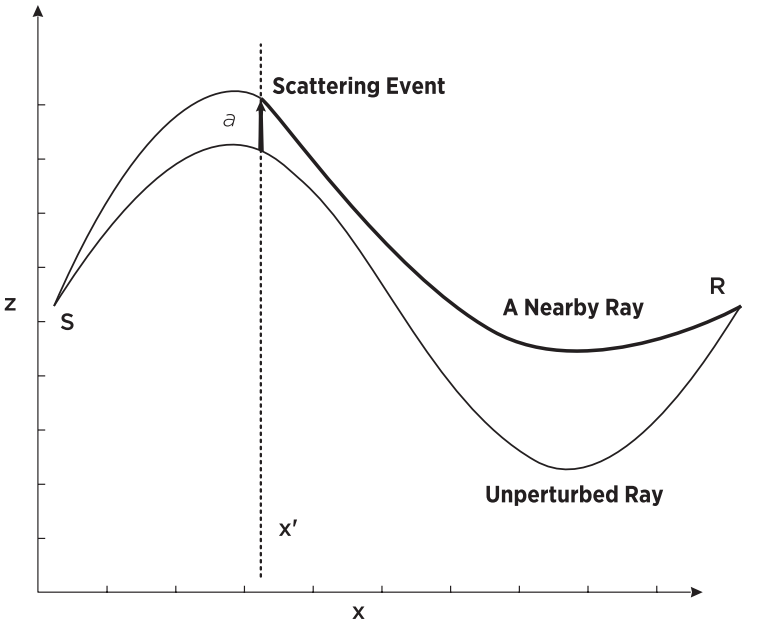

Figure 2.9. The Fresnel zone geometry for curved rays in a waveguide is shown. The broken ray at the scattering event is displaced vertically by a distance a.

Eq. 2.84 and expanding around the ray to second order gives the result

$$\Theta = \Theta_{ray} + q_0 \int_0^x \left[\frac{\dot{\xi}^2}{2} - \frac{\xi^2}{2} V''(z_r) \right] dx. \tag{2.85}$$

In Eq. 2.85 it is seen that the first-order terms disappear because the ray is an extremum of the travel time (Fermat's principle).

To compute the vertical Fresnel zone, consider a point at some intermediate range x' between the source and receiver that is displaced a vertical distance a from the unperturbed ray under consideration (see Figure 2.9). This new point $(x', z_r + a)$ helps define a new acoustic path connecting the source and receiver. This new path is actually composed of two rays obeying the ray equations: one propagating from the source to $(x', z_r + a)$ and the other joining $(x', z_r + a)$ to the receiver. At the range x' the new path has a discontinuity in slope that is sometimes interpreted as a virtual scatting event, but here it is clearly seen that the change in slope is necessary so that the path can end up at the receiver. Be that as it may the ray-tube functions ξ for these two displaced paths must be established. Because the ray-tube equation is a second-order equation the solution can be written as a linear combination of two solutions, namely

$$\xi(x) = c_1 \xi_1(x) + c_2 \xi_2(x),$$

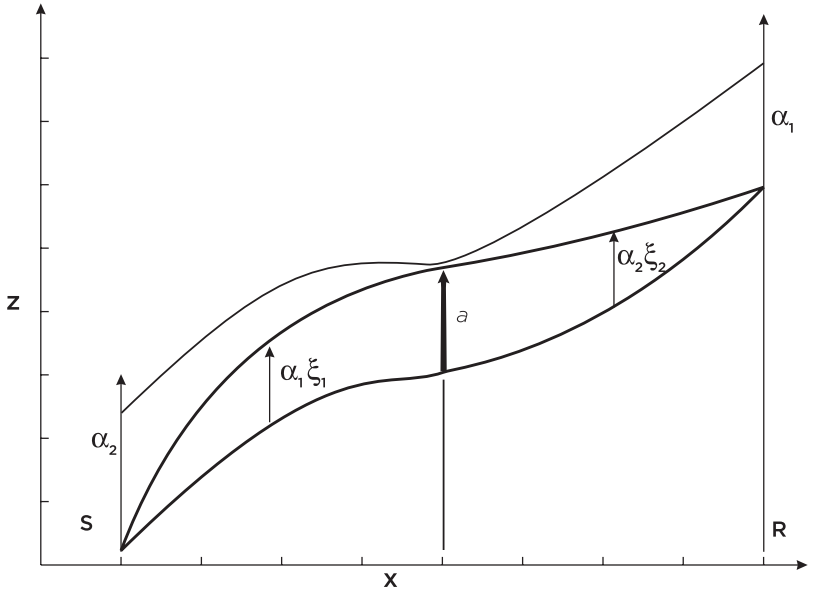

Figure 2.10. Geometry for the Fresnel zone construction from the ray tube functions ξ_1 and ξ_2.

where c_1 and c_2 are integration constants. To construct the ray tube functions it is useful to define the following boundary conditions for these solutions (see Figure 2.10),

$$\xi_1(0) = 0, \qquad \xi_1(R) = 1, \qquad \text{and} \qquad \xi_2(0) = 1, \qquad \xi_2(R) = 0.$$

Using the geometry in Figure 2.10, the displacement between the perturbed and unperturbed ray is

$$\alpha_1\xi_1(x) \qquad 0 < x < x', \qquad\qquad \alpha_2\xi_2(x) \qquad x' < x < R,$$

where α_1 and α_2 are now the two integration constants. Equating the solutions at x', gives

$$\alpha_1\xi_1(x') = \alpha_2\xi_2(x') = a. \tag{2.86}$$

Now the vertical Fresnel zone can be computed. Using Eq. 2.85 the difference in phase between the perturbed and unperturbed paths is given by

$$\Delta\Theta = q_0\left(\alpha_1^2\int_0^{x'}\left[\frac{\dot{\xi_1}^2}{2} - \frac{\xi_1^2}{2}V''(z_r)\right]dx + \alpha_2^2\int_{x'}^{R}\left[\frac{\dot{\xi_2}^2}{2} - \frac{\xi_2^2}{2}V''(z_r)\right]dx\right). \tag{2.87}$$

Using the ray tube equation and Eq. 2.86, the integrands in Eq. 2.87 can be written as total derivatives,[9] yielding the result

$$\Delta\Theta = q_0 \frac{a^2}{2}\left[\frac{\xi_2(x')\,\partial_x\xi_1(x') - \xi_1(x')\,\partial_x\xi_2(x')}{\xi_1(x')\xi_2(x')}\right]. \tag{2.88}$$

An important case is when the phase difference is equal to π such that there is destructive interference between the unperturbed and perturbed paths. The vertical distance a from the unperturbed path that results in this destructive interference is termed the first vertical Fresnel zone and its value is given by[10]

$$R_f(x') = \left[\lambda \frac{\xi_1(x')\xi_2(x')}{\xi_2(x')\,\partial_x\xi_1(x') - \xi_1(x')\,\partial_x\xi_2(x')}\right]^{1/2}. \tag{2.89}$$

Note here that the Fresnel zone scales as one over the square root of frequency. Appendix A describes the computational aspects of obtaining the Fresnel zone by integration along the ray path, and importantly if the receiver is too near a caustic this method will fail. It should also be remembered that Eq. 2.89 was obtained in the parabolic approximation and thus describes the Fresnel zone along a PE ray, not a Helmholtz equation ray. What is seen in most of the literature, however, is a hybrid of the PE and HE theories. The actual ray paths are found using the Helmholtz Hamiltonian and the PE ray tube equations are integrated along the HE rays. Recently an internally consistent procedure has been utilized (Colosi, 2015). Here the ray tube functions are computed using the Helmholtz Hamiltonian and the ray stability equation (Eq. 2.61). The key element of that equation for the ray tube is the quantity $q_{21} = \partial z/\partial p_0$, which gives the variation of the ray depth with initial ray slowness. The wide angle ray tube function is therefore $\xi = q_{21}\cos\theta_0/c_s$ where c_s is the sound speed at the source.

A few cases of special interest, in the PE approximation, can be easily calculated. First, for the case of a polar or constant sound-speed profile it is found that (see Appendix A)

$$R_f(x) = \left[\lambda \frac{x(R-x)}{R}\right]^{1/2}. \tag{2.90}$$

This constant sound speed Fresnel zone in fact is quite useful, not for the vertical direction but for the transverse directions around the ray where there is no waveguide. A second special case is for a parabolic sound-speed profile with the result that (again see Appendix A)

$$R_f(x) = \left[\lambda \left|\frac{\sin K_a x\ \sin K_a(R-x)}{K_a \sin K_a R}\right|\right]^{1/2}, \tag{2.91}$$

[9] The individual integrals are given by $\int_{x_1}^{x_2} \dot{\xi}^2 - \xi^2 V''\,dx = \xi\dot{\xi}\big|_{x_1}^{x_2}$.

[10] The denominator in the Fresnel zone equation is called the Wronskian and can be evaluated for any value of x'.

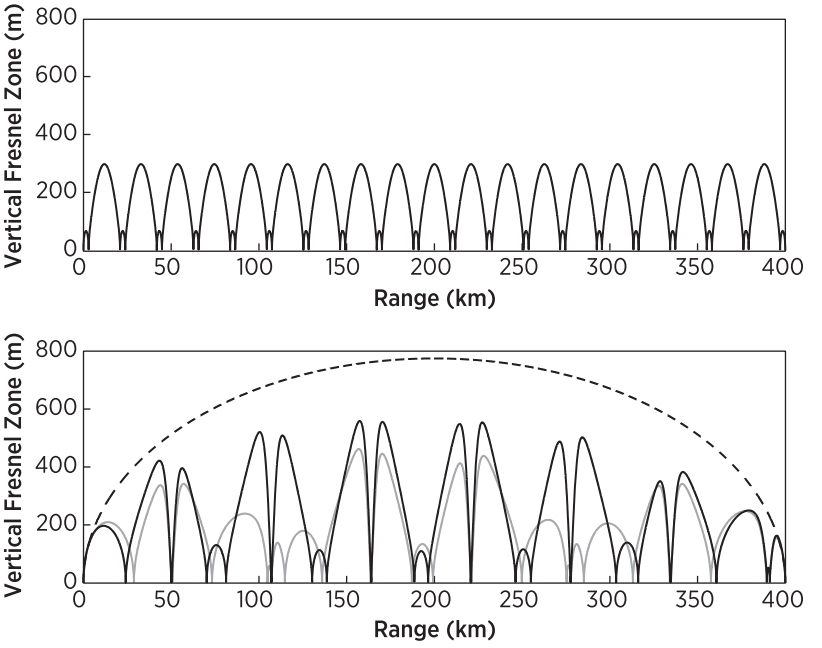

Figure 2.11. Vertical Fresnel zones in a Munk profile with the source on the axis for an axial ray (top) and near surface reflecting ray (bottom). The frequency is 250 Hz. For the axial ray the Fresnel zone is given by Eq. 2.91. For the high-angle ray, the Fresnel zone was computed using the ray tube equations in the parabolic approximation (gray) and using the variational equations (black). The constant sound speed Fresnel zone (dash) is shown for reference.

where $K_a = 2\pi/R_a = \sqrt{V''}$ is the horizontal wavenumber of the sinusoidal ray loop with double loop range R_a. This special case applies to rays traveling with small grazing angles near the deep sound-channel axis.

In general the Fresnel zone for mid-latitude or shallow-water profiles is more complicated than these special case expressions. Figure 2.11 shows the vertical Fresnel zone for 250-Hz propagation in the Munk profile for an axial ray and a near surface reflecting ray. For the axial ray a direct numerical calculation and Eq. 2.91 give identical results. For the high-angle ray a complicated variation of the Fresnel zone along the ray is evident, with zeros in the Fresnel zone where caustics exist (recall a caustic is where $\xi_1 = 0$). In the case of the high-angle ray, the Fresnel zone is computed using the PE ray tube equations and those from the variational equations. Differences in the two calculations occur because caustics are placed in different locations. Also shown in Figure 2.11 is the estimate of R_f from Eq. 2.90, and it is seen that the constant sound speed Fresnel zone roughly describes the envelope of the channeled ocean Fresnel zone.

2.6 Born and Rytov Approximations

Ray theory or geometrical acoustics provides a useful intuitive view of acoustic propagation through the stochastic internal-wave field, but as it has been seen there are important diffractive corrections that must be made especially near caustics. Later in this book, it will be found that the diffractive corrections will also be necessary due to the small-scale part of the internal-wave spectrum. In this section a perturbation method is introduced to account for the effects of diffraction in the regime in which acoustic fluctuations are small, though statistics of the wave field will not be treated (see later treatment in Chapter 6). Here it will be seen directly how the Fresnel zone enters into estimates of the acoustic pressure field.

Several inter-related methods have been applied to this situation, and are known as the Born approximation (Born and Wolf, 1999), the method of small perturbations (Tatarskii, 1971; Chernov, 1975), and the Rytov method (Rytov, 1937). Much of this work originated in the atmospheric optics context, in which line of sight propagation was considered through homogeneous isotropic turbulence. The seminal contributions in ocean acoustics were provided by Munk and Zachariasen (1976) and Flatté et al. (1979) in which the important effects of waveguide propagation and internal-wave inhomogeneity and anisotropy were correctly accounted for in the theory. In this book the Born approximation is used because it provides the simplest conceptual picture, and it provides similar accuracy to other weak fluctuation methods.

The analysis begins with the Helmholtz equation for the sound pressure field p at frequency ω, which can be written

$$\nabla^2 p + \bar{k}^2(z)\, p + 2q_0^2\, \mu(\mathbf{r})\, p \;=\; 0, \tag{2.92}$$

where $\bar{k} = \omega/\bar{c}(z)$, $q_0 = \omega/c_0$, $\mu = \delta c(\mathbf{r})/c_0$, and it is assumed $|\mu| << 1$. Using the well known Born approximation, consider the pressure field to be the sum of a series of ever-decreasing terms, where at each order n the order of smallness of the term is μ^n. This series may be convergent or divergent, depending on the magnitude of μ; however, an important physical interpretation of the series terms is that of multiple scattering. The zero-order term represents the unperturbed wave, the first-order term represents single scattering, the second double scattering, and so on. Writing the series as $p = p_0 + p_1 + p_2 + \cdots + p_n$, substituting into Eq. 2.92 and equating terms of equal order the result is

$$\nabla^2 p_0 + \bar{k}^2(z)\, p_0 = 0, \tag{2.93}$$

$$\nabla^2 p_1 + \bar{k}^2(z)\, p_1 = -2q_0^2\, \mu\, p_0, \tag{2.94}$$

etc....

In the present treatment, in which the concern is weak fluctuations, all terms of order higher than 1 will be ignored. In this single scattering approximation, it is important to note that the equation has been transformed from one in which there is a multiplicative randomness which is a difficult problem to solve (e.g., Eq. 2.92) to one in which there is an additive randomness that is quite easily solved (e.g., Eq. 2.94). That is to say, in Eq. 2.94 the left-hand side of the equation (i.e., the deterministic component) is driven on the right-hand side of the equation by the random function $\mu\ p_0$ alone which does not involve p_1. In this case an explicit solution is available for p_1, which is simply the convolution of the Green's function with the right-hand side of the equation,

$$p_1(\mathbf{r}) = -\int_V d^3\mathbf{r}' G(\mathbf{r},\mathbf{r}')\Big[2q_0^2\,\mu(\mathbf{r}')\ p_0(\mathbf{r}')\Big]. \tag{2.95}$$

This equation tells us that the scattered field observed at location $\mathbf{r}$ has a contribution from scattered waves at all locations in space $\mathbf{r}'$. That is to say, the unperturbed wave propagates to location $\mathbf{r}'$, where it is scattered with strength $2q_0^2\ \mu(\mathbf{r}')\ p_0(\mathbf{r}')$. This wave then propagates via the Green's function from $\mathbf{r}'$ to the observation location $\mathbf{r}$, where the total pressure field p_1 is the sum over all the scattered waves. In ocean acoustics where there is multipath propagation one must conceptually consider this process to occur locally near a particular ray path. Thus it should be understood that all locations in space will not contribute equally to the scattered wave; in particular it will be found that there is a distinct region around the unperturbed ray path from which the dominant contributions come. This is the Fresnel zone.

The significance of the Fresnel zone can be better appreciated by examining propagation without a waveguide. In this case the free space Green's function is $G(\mathbf{r},\mathbf{r}') = \exp(iq_0|\mathbf{r}-\mathbf{r}'|)/(4\pi|\mathbf{r}-\mathbf{r}'|)$, and an initial point source $p_0(\mathbf{r}) = \exp(iq_0|\mathbf{r}|)/(4\pi|\mathbf{r}|)$ is used. For the observation point at $\mathbf{r} = (R,0,0)$, that is a ray along the x-axis, the Born pressure field under the small-angle scattering approximation[11] is (Colosi, 1999)

$$p(\mathbf{r}) = p_0(\mathbf{r})\Big[1 - q_0\int_0^R dx' \int_{-\infty}^{\infty}\int_{-\infty}^{\infty} \frac{dy'dz'}{R_f^2(x')}\,\mu(\mathbf{r}')\exp\Big[i\pi\frac{(y'^2+z'^2)}{R_f^2(x')}\Big]. \tag{2.96}$$

Here it is seen that for $y' > R_f$ and $z' > R_f$ the exponential term will be rapidly oscillating and will not contribute to the pressure. On the other hand, for y' and z' smaller than the Fresnel radius there will be reinforcing contributions to the pressure. The Fresnel zone thus describes a region around the ray that has

[11] In the small-angle scattering approximation the relative distance is Taylor expanded so that $|\mathbf{r}-\mathbf{r}'| \simeq (R - x')[1 + (y'^2 + z'^2)/(2(R-x')^2)]$.

significant influence on the observed pressure. This topic and the results for various moments of the acoustical field will be discussed in Chapters 4 and 6.

2.6.1 Relation to Amplitude and Phase

Here it is shown how Eq. 2.95 describes the relative fluctuations of phase and amplitude. Writing the ratio of total pressure to the unperturbed pressure gives

$$\frac{p_T}{p_0} = 1 + \frac{p_1}{p_0} = \frac{A_0 + A_1}{A_0}\, \mathrm{e}^{i(\phi_T - \phi_0)}, \tag{2.97}$$

where $p_0 = A_0 \mathrm{e}^{i\phi_0}$, $p_1 = A_1 \mathrm{e}^{i\phi_1}$, and $p_T = p_0 + p_1 \simeq (A_0 + A_1)\mathrm{e}^{i\phi_T}$ because ϕ_1 is nearly equal to ϕ_0. Taking the natural log of the ratio of pressures then gives

$$\ln\left(1 + \frac{p_1}{p_0}\right) = \ln\left(1 + \frac{A_1}{A_0}\right) + i(\phi_T - \phi_0). \tag{2.98}$$

Because p_1 is a small correction to p_0, the log can be expanded in a power series and to first order the result is

$$\frac{p_1}{p_0} \simeq \frac{A_1}{A_0} + i(\phi_T - \phi_0). \tag{2.99}$$

Thus it is seen that the real part of Eq. 2.95 gives the relative amplitude fluctuation, while the imaginary part gives the relative phase fluctuation. Often the concern is the log-amplitude fluctuation, namely $\chi = \ln(A/A_0)$, but from above it is seen that $\chi \simeq A_1/A_0$.

2.6.2 Relationship between Born and Rytov Solutions

The Born approximation is often contrasted to the method of Rytov in which the pressure is expanded in an exponential series. For the Rytov method one writes $p(\mathbf{r}) = \exp(\varphi_0 + \varphi_1 + \varphi_2....) = \exp(\varphi)$, and substituting this into the Helmholtz equation gives

$$\nabla^2\varphi + (\boldsymbol{\nabla}\varphi)^2 + \bar{k}^2(z) - q_0^2\mu = 0. \tag{2.100}$$

Equation 2.100 is nonlinear and is known as the Riccati equation. To zeroth and first order the Riccati equation gives

$$\nabla^2\varphi_0 + (\boldsymbol{\nabla}\varphi_0)^2 + \bar{k}^2(z) = 0, \tag{2.101}$$

$$\nabla^2\varphi_1 + 2\boldsymbol{\nabla}\varphi_0 \cdot \boldsymbol{\nabla}\varphi_1 = 2q_0^2\mu. \tag{2.102}$$

The zeroth order equation has a solution $p_0 = \exp(\varphi_0)$, which is the solution to the unperturbed problem. To solve the first-order equation one writes $\varphi_1 = \exp(\varphi_0)u$

and substituting this into the equation gives

$$\nabla^2 u + q_0^2 u = 2q_0^2 \mu \exp(\varphi_0). \tag{2.103}$$

The solution to the first-order equation can then be written

$$\varphi_1 = \exp(\varphi_0)u = -\int_V d^3\mathbf{r}' G(\mathbf{r},\mathbf{r}')\left[2q_0^2\,\mu(\mathbf{r}')\,\frac{p_0(\mathbf{r}')}{p_0(\mathbf{r})}\right]. \tag{2.104}$$

It can be easily shown that the Born and Rytov results are related by

$$p^{Rytov}(\mathbf{r}) = p_0(\mathbf{r})\mathrm{e}^{p_1(\mathbf{r})/p_0(\mathbf{r})} \simeq p_0\left(1+\frac{p_1}{p_0}\right) = p_0 + p_1 = p^{Born}(\mathbf{r}), \tag{2.105}$$

where the approximation in this equation comes from a Taylor series expansion of the exponential, which is clearly valid if $p_1/p_0 << 1$. Therefore the Born and Rytov results are the same when $p_1/p_0 << 1$, which is the requirement for both perturbation expansions to be valid. While some texts claim that the Rytov result is superior to the Born result, it is clear that these claims are unfounded.

2.7 Path Integrals

The path integral has been shown to be a solution of the parabolic wave equation, and though technically sophisticated in execution (see Feynman and Hibbs, 1965), the conceptual picture of the path integral is actually quite simple. Given a source and a receiver, the acoustic field observed at that receiver will be a sum over *all* the possible acoustic paths that start at the source and end at the receiver. This approach could be considered a generalization of Huygens principle. At first glance the task of summing up this infinite set of paths seems unduly onerous, but what has been discovered is that in some cases there is a significantly smaller subset of these paths that are actually important. In fact it is those paths that lie within a few Fresnel zones of the unperturbed ray path.

With these ideas in mind, the introduction to the path integral method is started by considering the variational approach to ray propagation, that is, a method of ray analysis often associated with "Fermat's principle" or the "principle of least time."

2.7.1 Variational Approach to Ray Propagation

It is well known that many of the laws of physics can be expressed in terms of variational principles, an example of which is Newton's laws of motion, which can be derived from the principle of least action (Landau and Lifshitz, 1976). In wave propagation the principle of least time, or more generally the principle that the travel time is an extremum (Gutzwiller, 1990), can be used to derive the ray

trajectory. For a general 3-D path connecting the source and receiver, the travel time along that path is written

$$T(path) = \int_{path} L(z,x)\,ds, \tag{2.106}$$

where $ds = (dx^2 + dy^2 + dz^2)^{1/2} = (dx_i dx_i)^2$ is an infinitesimal path length increment, and the convention of summing over repeated indicies is used. The Lagrangian density function is given by $L = 1/c(x,z)$, thus giving the familiar ray travel time equation. To examine how the travel time changes when the path is changed, the variation of Eq. 2.106 is calculated, yielding

$$\delta T = \int_{path} (ds\delta L + L\delta ds) = \int_{path} \left(\delta x_i \frac{\partial L}{\partial x_i} + L\dot{x}_i \delta d\dot{x}_i\right) ds, \tag{2.107}$$

where an overdot represents differentiation with respect to s and the result that $\delta ds = dx_i \delta dx_i/ds = \dot{x}_i \delta d\dot{x}_i ds$ has been used. There is a useful physical interpretation of Eq. 2.107. The first term in the integral represents the change in travel time due to a change in the speed of sound over the path, and the second term represents the change in travel time due to the changing path length. The second term can be simplified using integration by parts, noting that the boundary terms are zero since the path perturbations must vanish at the source and receiver. The result is

$$\delta T = \int_{path} \delta x_i \left[\frac{\partial L}{\partial x_i} - \frac{d}{ds}(L\dot{x}_i)\right] ds. \tag{2.108}$$

Now if it is asserted that the variation in travel time around the "real" path taken by the sound is zero (i.e., Fermat's principle), then this condition requires the quantity in the square brackets of Eq. 2.108 to be zero. The Euler-Lagrange equations or ray equations (in vector form) result giving

$$\ddot{\mathbf{x}} = \frac{\boldsymbol{\nabla} L}{L} - \dot{\mathbf{x}}\left(\dot{\mathbf{x}} \cdot \frac{\boldsymbol{\nabla} L}{L}\right). \tag{2.109}$$

The vector $\dot{\mathbf{x}}$ is pointing in the direction of the ray, and the second term on the right-hand side of the equations is just the projection of the gradient of L in the direction of the ray. Thus Eq. 2.109 says that the change in direction of the ray $\ddot{\mathbf{x}}$ is affected only by the sound-speed gradients perpendicular to the direction of the ray; this is precisely the result that will be obtained from weak fluctuation theory (see Chapter 6). This equation can be interpreted more easily if 2-D propagation in the (x,z) plane is examined. In this case $ds = dx/\cos\theta$ and $\tan\theta = dz/dx$ so that the ray equations become

$$\frac{d\theta}{dx} = \tan\theta \frac{1}{c}\frac{\partial c}{\partial x} - \frac{1}{c}\frac{\partial c}{\partial z}. \tag{2.110}$$

In the case of small-angle propagation this equation reduces to

$$\frac{d\theta}{dx} + \frac{1}{c_0}\frac{\partial c}{\partial z} = 0, \tag{2.111}$$

where the factor of c in the denominator has been replaced by c_0. Using $\theta \simeq dz/dx$ the PE ray equation

$$\frac{d^2z}{dx^2} + \frac{1}{c_0}\frac{\partial c}{\partial z} = 0, \tag{2.112}$$

is recovered (see Eqs. 2.47 and 2.48).

2.7.2 Path Integrals: A Qualitative Discussion

It is now appreciated how ray theory comes out of a variational principle related to the sound energy path, but it is also known from previous discussions of the Fresnel zone that one cannot consider the ray to be infinitely thin; there is some region of paths around the ray that are important due to diffractive effects. The path integral formalism allows us to use this physical picture in a meaningful way such that the acoustical pressure at frequency ω is written

$$p(\mathbf{x}) = N \int d(path) \exp\Big(i\Theta(path)\Big), \tag{2.113}$$

where the integration is over all paths connecting the source and receiver ($\mathbf{x} = (R, y, z)$), Θ is the accumulated phase over the path, and the factor N is a normalization. If the case is considered in which the sound speed is only a function of depth then the primary contributions to p will be from paths within a Fresnel zone of the equilibrium or unperturbed ray. Recall that paths within a Fresnel zone arrive at the receiver with a phase less than a half cycle of the equilibrium ray phase and are thus not prone to interference or cancellation.

So, to get a better feeling for the path integral method, the form of the path integral that is useful for ocean acoustics purposes is presented, and the conceptual picture of the path integral is further developed. Application of path integrals to the specific cases with internal-wave-induced sound-speed perturbations will be deferred until Chapter 7.

2.7.3 Formulation of the Path Integral

The path integral method in ocean acoustics has been exclusively applied in cases for which the parabolic approximation can be made. In this approximation the Lagrangian density is given by (Flatté et al., 1979) (also see Eq. 2.84)

$$L\left(\frac{\partial y}{\partial x}, \frac{\partial z}{\partial x}, x, y, z\right) = \frac{1}{c_0}\left[\frac{1}{2}\left(\frac{\partial y}{\partial x}\right)^2 + \frac{1}{2}\left(\frac{\partial z}{\partial x}\right)^2 - U(z) - \mu(x, y, z)\right], \tag{2.114}$$

where it has been written $V \simeq U(z) + \mu(\mathbf{r})$ with $\bar{c}(z) = c_0(1 + U(z))$. This form is particularly pleasing because the path integral can be written as the product of two parts, one dependent on the unperturbed phase and the other due to the fluctuations. In order to simplify the notation the path integral Eq. 2.113 is written as

$$p(\mathbf{r}) = N \int d(path) \exp\left(i\Theta_0(path) - iq_0 \int_0^R \mu(x, y(x), z(x))\, dx\right), \tag{2.115}$$

where the unperturbed phase Θ_0 associated with the path is

$$\Theta_0(path) = q_0 \int_0^R \left[\frac{1}{2}\left(\frac{\partial y}{\partial x}\right)^2 + \frac{1}{2}\left(\frac{\partial z}{\partial x}\right)^2 - U(z)\right] dx. \tag{2.116}$$

Here the factor $N^{-1} = \int d(path) e^{i\Theta_0(path)}$ is a normalization so the $p = 1$ for $\mu = 0$.

2.7.4 Solution of the Parabolic Equation as a Path Integral

It can be shown that the solution of the parabolic wave equation can be written as a path integral (Flatté et al., 1979), that is

$$A(\mathbf{x}) = \int d(\text{paths})\, \mathrm{e}^{i\Theta_0(\text{path})}. \tag{2.117}$$

To understand this result it is useful to look at the parabolic equation, 2.11, in discretized form,

$$\begin{aligned} \frac{A(x+d,z) - A(x,z)}{d} &= \left[\frac{i}{2q_0}\frac{\partial^2}{\partial z^2} - iq_0 U\right] A(x,z), \\ A(x+d,z) &= \left(1 + i\left[\frac{1}{2q_0}\frac{\partial^2}{\partial z^2} - q_0 U\right] d\right) A(x,z), \\ &\simeq \exp\left(\frac{id}{2q_0}\frac{\partial^2}{\partial z^2}\right) \hat{A}(x,z), \end{aligned} \tag{2.118}$$

where d is the range step and the waveguide, phase shifted wave function is $\hat{A}(x,z) = \mathrm{e}^{-iq_0 U d} A(x,z)$. Next it is recognized that Eq. 2.118 can be solved by transforming to the Fourier domain thus,

$$A(x+d, k_z) = \exp\left(-i\frac{k_z^2 d}{2q_0}\right) \hat{A}(x, k_z). \tag{2.119}$$

To complete the solution, $A(x+d,z)$ is then obtained by inverse Fourier transform. Here the exponential factor in Eq. 2.119 is termed the free propagator, and the exponential term in $\hat{A}$ is called the phase screen. Physically the transformation of the wave function from x to $x+d$ can be understood as being accomplished in two steps:

1. The first step is the phase screen in which the accumulated phase advance across the step d by the sound-speed structure is accounted for.
2. The second step is the propagation of the phase shifted wave function across the horizontal distance d using the free space propagator.

The relation to the path integral can now be clearly seen by writing out explicitly the FFT relations,

$$A(x+d,z) = \frac{1}{\sqrt{2\pi}} \int_{-\infty}^{\infty} dk_z e^{ik_z z}\, e^{-ik_z^2 d/(2q_0)} \int dz'\, e^{-ik_z z'} \hat{A}(x,z'),$$

$$= \sqrt{\frac{q_0}{id}} \int dz' \hat{A}(x,z') \exp(iq_0(z-z')^2/(2d)),$$

$$= \sqrt{\frac{q_0}{id}} \int dz' \hat{A}(x,z') \exp(i\Theta_0(x,z',x+d,z)), \tag{2.120}$$

$$\Theta_0(x,z',x+d,z) = q_0(d^2+(z-z')^2)^{1/2} - q_0 d \simeq q_0 \Delta z^2/(2d), \tag{2.121}$$

where the k_z integral was done by completing the square in the exponent. Note that for the unperturbed phase one must account for the $e^{iq_0 d}$ term used to derive the PE. Importantly, Eq. 2.120 shows that the value of the wave function at $(x+d,z)$ is the integral of all the linear paths (free space) that connect the phase shifted wave function $\hat{A}(x,z')$ to the final point $A(x+d,z)$. For finite d the operations explained here correspond to solution by numerical methods, and for infinitesimal d, one obtains the solution of the parabolic wave equation. In either case the operations described here demonstrate the method of *Path Integrals*.

As in the case for rays and the Born method in this chapter, here is where the matter will be left for now. In Chapter 7 the issue of internal waves and path integrals will be taken up in detail.

2.8 Normal Modes

Using the method of rays one is able to understand geometrically the structure of wave fronts in the ocean sound channel. Given an impulsive source, one expects a series of delta-like arrivals of ever-increasing amplitude (a crescendo) until a final cut off. However, the arrival pattern is necessarily more complex than this due to both interference effects between arrivals and diffraction. To address the issue of interference and diffraction, the Born approximation and the method of path integrals have been described. Continuing in this spirit, the method of acoustic normal modes is introduced.

The normal mode approach to ocean acoustic propagation has proven to be a powerful tool for describing both deep-water and shallow-water problems, and its application to transport theory for sound propagation through the stochastic internal-wave field has provided ocean acousticians with perhaps the most accurate model to date. While ray and path integral methods have an elegant physical interpretation, mode methods are more algebraic and abstract due to the fact that only a sum over modes provides real physical information. In this section the deterministic theory of normal modes applied to ocean acoustics will be developed, and the interested reader who wants to delve deeper into the subject is referred to the ample reference material on this topic (see Frisk, 1994; Jensen et al., 1994; Munk et al., 1995).

2.8.1 Coupled Mode Equations

The coupled mode equations are easily derived from the wave equation when 2-D propagation in the depth-range plane is considered. The treatment of 3-D effects is somewhat more cumbersome, and a brief account is given at the end of this section (Penland, 1985; Voronovich and Ostashev, 2006). The starting place is close to Eq. 2.92, but because there is interest in applying the normal mode approach in both deep and shallow-water environments the background density profile denoted as $\rho_0(z)$ is retained. In cylindrical coordinates the Helmholtz equation becomes

$$\frac{1}{r}\frac{\partial}{\partial r} r \frac{\partial p}{\partial r} + \rho_0(z)\frac{\partial}{\partial z}\left(\frac{1}{\rho_0(z)}\frac{\partial p}{\partial z}\right) + \bar{k}^2(z)p = 2q_0^2 \mu p. \tag{2.122}$$

For the fluctuation problem it is expedient to expand the pressure in terms of the modes of the unperturbed problem so that

$$p(r,z;\omega) = \sum_n \frac{a_n(r)\,\phi_n(z)}{\sqrt{k_n r}}, \tag{2.123}$$

where

$$\rho_0(z)\frac{\partial}{\partial z}\left(\frac{1}{\rho_0(z)}\frac{\partial \phi_n}{\partial z}\right) + \left(\bar{k}^2(z) - k_n^2\right)\phi_n = 0, \tag{2.124}$$

is the unperturbed mode equation for the eigenmodes ϕ_n and eigenwavenumbers k_n. The boundary conditions for the mode equation are $\phi_n(0) = 0$, and continuity of pressure and normal velocity at the water/seafloor interface (depth D) or other layers in the bottom. The modes obey the othonormality relation

$$\int_0^\infty \frac{\phi_n(z)\phi_m(z)}{\rho_0(z)} dz = \delta_{mn}. \tag{2.125}$$

It is important to note that in the treatment of mode scattering by internal waves the primarily concern will be with the behavior of *trapped* modes, that is the modes

with discrete mode numbers that are confined by the ocean waveguide and sea surface. In principle the *continuum* modes that are also a solution of Eq. 2.124 could be used, but because these modes are not confined by the ocean waveguide they tend to attenuate quickly and become irrelevant.

Note here that due to the use of the unperturbed mode function basis all the variability due to sound-speed fluctuations is captured in the mode amplitude term $a_n(r)$. This formulation will prove quite useful when addressing acoustic field statistics.

In the mode approach the second-order partial differential equation of Eq. 2.122 can be reduced to a set of coupled ordinary differential equations. This objective is accomplished by substituting Eq. 2.123 into Eq. 2.122, multiplying the resulting equation by ϕ_m/ρ_0 and integrating over depth. The final result (switching the m and n indices) is

$$\frac{d^2 a_n}{dr^2} + k_n^2 a_n = 2k_n \sum_m a_m \rho_{mn}(r), \tag{2.126}$$

where

$$\rho_{mn}(r) = \frac{q_0^2}{\sqrt{k_n k_m}} \int_0^\infty \frac{\phi_n(z)\phi_m(z)}{\rho_0(z)} \mu(r,z)\, dz, \tag{2.127}$$

is the symmetric coupling matrix. When $\mu = 0$ then $\rho_{mn} = 0$ and solution of Eq. 2.126 gives the expected plane wave result $a_n(r) = a_n(0)\exp(\pm ik_n r)$. A few general statements can be made about the coupling matrix. First, this matrix tells us how strongly mode n is coupled to mode m. Because $|\mu| << 1$ in the ocean there is small-angle scattering. Since coupling from mode n to m physically represents a change in the vertical angle, then small-angle scattering implies that the coupling matrix will be strongly peaked along the diagonal, that is to say, near-neighbor coupling will be dominant. In the next section on the adiabatic approximation, it will be shown that the diagonal elements of the coupling matrix physically represent local perturbations to the modal wavenumber. Lastly, it is seen that Eq. 2.127 scales approximately as acoustic frequency; thus coupling is expected to be strongest for high frequency.

It is seen that Eq. 2.126 is a second-order equation and thus admits both forward and backscattered waves. Since internal-wave-induced sound-speed perturbations cause small-angle forward scattering it is useful to convert to a one-way equation. It is also useful to remove the rapid oscillations in the mode amplitude function. To accomplish both these objectives one writes $\hat{a}_n = a_n e^{-ik_n r}$ and this is substituted into Eq. 2.126. To an excellent approximation the phase variation of the mode amplitude is much more rapid than the amplitude variation; thus the second-order

range derivative term can be ignored yielding (Dozier and Tappert, 1978a)

$$\frac{d\hat{a}_n}{dr} = -i \sum_m \hat{a}_m \, \mathrm{e}^{ik_{mn}r} \, \rho_{mn}(r), \tag{2.128}$$

where $k_{mn} = k_m - k_n$. The re-modulated equation is also of use so it is written down here for completeness.

$$\frac{da_n}{dr} - ik_n a_n = -i \sum_m a_m \rho_{mn}(r). \tag{2.129}$$

The effects of attenuation on coupled mode behavior have been addressed by a few investigators (see Dozier, 1983; Creamer, 1996; Colosi, 2008). In this case the modal wavenumber has a small complex component that is defined as $l_n = k_n + i\alpha_n$, where α_n is generally computed using perturbation theory,

$$\alpha_n = \frac{\omega}{k_n} \int_0^\infty \frac{\alpha(z)}{\bar{c}(z)} \frac{\phi_n^2(z)}{\rho_0(z)} dz. \tag{2.130}$$

In Eq. 2.130 the quantity $\alpha(z)$ is the complex part of the total wavenumber $k(z) = \omega/\bar{c}(z) + i\alpha(z)$. Modal attenuation is critical for shallow-water problems due to the acoustic interaction with the lossy seafloor. In deep-water cases attenuation can be a factor if the acoustic frequency is sufficiently high, or if some bottom interaction exists (e.g., bottom limited propagation). In shallow-water situations, modal attenuation is generally higher for low frequencies and higher mode numbers since in both these cases the modes tend to penetrate further into the lossy seabed. For weak attenuation the coupled mode equations become to first order (Dozier, 1983; Creamer, 1996)

$$\frac{d\hat{a}_n}{dr} = -i \sum_{m=1}^{N} \rho_{mn}(r) \mathrm{e}^{il_{mn}r} \hat{a}_m(r). \tag{2.131}$$

Here the coupling matrix ρ_{mn} is unchanged to first order, and the difference wavenumber is now, $l_{mn} = k_{mn} + i\alpha_{mn}$, with $\alpha_{mn} = \alpha_m - \alpha_n$. In the absence of attenuation Eq. 2.128 conserves energy (Dozier and Tappert, 1978a), but with the complex wavenumber it is found that

$$\frac{d}{dr} \sum_n |\hat{a}_n|^2 = \sum_n \hat{a}_n \frac{d\hat{a}_n^*}{dr} + \hat{a}_n^* \frac{d\hat{a}_n}{dr} \simeq -\sum_n 2\alpha_n |\hat{a}_n|^2. \tag{2.132}$$

The analysis just presented can also be carried out for 3-D propagation primarily in the r direction (i.e., small horizontal angle scattering) in which the modes can couple in both the range and cross range directions. The result for $\hat{a}_n(r, y)$, which

is simply quoted here gives

$$\frac{\partial \hat{a}_n}{\partial r} + \frac{1}{2ik_n}\frac{\partial^2 \hat{a}_n}{\partial y^2} = -i\sum_m \rho_{mn}(r,y)\, \mathrm{e}^{il_{mn}r}\, \hat{a}_m, \tag{2.133}$$

where

$$\rho_{mn}(r,y) = \frac{q_0^2}{(k_m k_n)^{1/2}} \int_0^D \frac{\phi_n(z)\phi_m(z)}{\rho_0(z)} \mu(r,y,z)\, dz. \tag{2.134}$$

The solution of this equation poses a much more difficult task. Because the horizontal gradients of internal waves are relatively weak, the cross range coupling is generally assumed to be significant only at extremely long range and high frequency (Penland, 1985); however this issue remains an open scientific question (Voronovich and Ostashev, 2006).

The mode equations represent an initial value problem, dictating the evolution of the mode amplitude from the initial conditions. The mode amplitude initial condition can be derived from an initial acoustic pressure distribution $p(r=0,z)$, such that

$$a_n(0) = \int_0^\infty p(r=0,z)\frac{\phi_n(z)}{\rho_0(z)} dz. \tag{2.135}$$

For a point source at depth z_s with $p(r=0,z) = \delta(z-z_s)$, the initial mode amplitude is $a_n(0) = \phi_n(z_s)/\rho_0(z_s)$.

2.8.2 Adiabatic Theory

A surprisingly useful solution to the coupled mode equations can be obtained using the adiabatic approximation. In the adiabatic approximation the coupling matrix is assumed to be so strongly peaked along the diagonal that mode coupling is insignificant and the equations are essentially uncoupled. Several conditions have been derived to denote the regime of validity of the adiabatic approximation (Milder, 1969), none of which have proved terribly useful in the study of sound transmission through ocean internal waves. Suffice it to say the approximation is generally better for lower acoustic frequencies, but some caution is warranted when using the approximation, and testing is recommended. The adiabatic mode amplitude is given by

$$a_n(r) = a_n(0)\mathrm{e}^{il_n r} \exp\left(-i\int_0^r \rho_{nn}(r')dr'\right), \tag{2.136}$$

where $a_n(0)$ is the initial mode amplitude at the source. Here the diagonal of the coupling matrix is seen to physically represent a local wavenumber perturbation, that is, the total local wavenumber is $k_n - \rho_{nn}(r)$. This effect can also be interpreted

as a local speeding up/slowing down of the mode. These adiabatic modal phase fluctuations can be contrasted to phase fluctuations induced by mode coupling. In many cases, as will be discussed later, the adiabatic phase fluctuations constitute an equal or dominate contribution to modal phase randomization, especially in shallow-water situations.

2.8.3 Vertical Modes, Horizontal Rays

The subject of vertical modes and horizontal rays was introduced into the ocean acoustics literature by Weinburg and Burridge (1974). The physical picture is that adiabatic mode theory applies in the vertical, but the modes can refract horizontally. This means that vertical changes in angle are assumed small but horizontal angle changes are not. Using Eq. 2.133 with the adiabatic approximation yields the horizontal wave equation for mode n (Wolfson and Tappert, 2000)

$$\frac{i}{k_n}\frac{\partial \hat{a}_n}{\partial r} = -\frac{1}{2k_n^2}\frac{\partial^2 \hat{a}_n}{\partial y^2} + \frac{\rho_{nn}(r,y)}{k_n}\hat{a}_n. \tag{2.137}$$

Note that this equation has the same form as the parabolic equation, and the mode rays are seen to propagate through the random wavenumber perturbation field $\rho_{nn}(r,y)$. Introducing the mode phase velocity $c_p(n) = \omega/k_n$, a useful ray Hamiltonian function akin to Eq. 2.46, is given by

$$H = \frac{c_p(n)p_y^2}{2} + \frac{\mu_p(n,r,y)}{c_p(n)}, \tag{2.138}$$

where $\rho_{nn}(r,y)/k_n \simeq \delta c_p(n,r,y)/c_p(n) = \mu_p(n,r,y)$ and the canonical variables are $(y, p_y = \tan\vartheta/c_p(n))$ with ϑ being the horizontal angle. From this Hamiltonian function all information concerning the ray structure of $\hat{a}_n$ can be derived (see Section 2.4). It is important to point out that the physical interpretation of the mode rays is different from that of the "classical" rays and their associated wave fronts. Here the rays do not travel at the local group speed, but roughly at the local phase speed. It is not exactly the phase speed because the small-angle approximation has been made. In order to compute wave front quantities in the ray-mode approach, the fields must be computed for a range of frequencies and subsequently Fourier synthesized to create a wave front.

The vertical mode, horizontal ray approach has been used to study acoustic scattering by ocean mesoscale structure (Wolfson and Tappert, 2000). While the technique has not been applied in the study of stochastic internal-wave scattering, it could be a useful tool to understand 3-D scattering effects. The technique in slightly different form than presented here has found wide application in global-scale acoustics (Heaney et al., 1991; Dushaw, 2008), shallow-water acoustic propagation through nonlinear internal-wave packets (Katznelson and

Pereselkov, 2000; Lynch et al., 2010; Katznelson et al., 2012), and in basin-scale internal tide propagation studies (Rainville and Pinkel, 2006).

2.8.4 Modes in a Range-independent Ocean

The modal acoustic field in the case of a range-independent sound-speed profile provides important information from which to judge the effects of internal waves. The structure of the wave front, shadow zones, and interference patterns will all be altered by the scattering effects of internal waves, and so the subject of a range-independent ocean is briefly examined.

When sound speed is only a function of depth, the Helmholtz equation is separable, allowing us to write (Jensen et al., 1994)

$$p(r,z;\omega) = \frac{i}{4}\sum_n a_n(0)H_0^1(l_n r)\phi_n(z), \tag{2.139}$$

where H_0^1 is the Hankel function. For most cases the asymptotic form of the Hankel function is adequate, and one can write

$$H_0^1(l_n r) \simeq \sqrt{\frac{2}{\pi k_n r}}\mathrm{e}^{i(l_n r-\pi/4)}, \tag{2.140}$$

where the requirement is $k_n r >> 1$ and $\alpha_n << k_n$. For a point source, to acquire TL one simply normalizes by the pressure at $r = 1$ m, using the spherical wave $p_0(r) = \mathrm{e}^{ik_s r}/(4\pi r)$ where $k_s = \omega/c_s$. For single-frequency the result is $TL = -20\log_{10}(|p(r,z;\omega)|/|p_0(r=1;\omega)|)$.

For transient signals an integration over frequency is required so that

$$p(r,z,t) = \sum_n p_n(r,z,t), \tag{2.141}$$

$$p_n(r,z,t) = \int_{-\infty}^{\infty} W(\omega)a_n(0;\omega)H_0^1(l_n r;\omega)\phi_n(z;\omega)\mathrm{e}^{-i\omega t}d\omega, \tag{2.142}$$

where $W(\omega)$ is the source frequency response function. The quantity $p_n(r,z,t)$ is referred to as the mode pulse, that is, the time arrival pattern for mode n. The mode pulse has garnered some attention as an observable for ocean acoustic tomography (Munk et al., 1995), and its stability in the presence of stochastic internal waves has also been investigated (Colosi and Flatté, 1996; Udovydchenkov and Brown, 2008; Udovydchenkov et al., 2012). With regard to broadband TL, a point source normalization similar to the single-frequency case is used, except here the peak pressure for the spherical wave $p_0(r,t)$ at a one-meter range is used.

Modal phase and group velocities are important quantities that can be treated simply in the range-independent case. These horizontal velocities are defined as

$$c_p(n) = \frac{\omega}{k_n}, \qquad c_g(n) = \frac{d\omega}{dk_n}. \tag{2.143}$$

They are closely related to the ray loop horizontal velocities discussed in Section 2.4.6. A useful expression for the group speed is the Rayleigh formula (Munk et al., 1995)

$$c_g(n)c_p(n) = \left(\int_{-\infty}^{0} \frac{1}{c^2(z)} \frac{\phi_n^2(z)}{\rho_0(z)} dz \right)^{-1}. \tag{2.144}$$

Modal Structure and Kinematics

Because the coupled mode equations have been written in terms of the modes in the range-independent ocean, these eigenmodes and eigen-wavenumbers will play a critical role in the theory of acoustic fluctuations and they dictate the sensitivity of the acoustic field to the various scales of sound-speed structure in the ocean. In particular, the shape of the modes $\phi_n(z)$ relative to the vertical distribution of sound-speed fluctuation variance $\langle \mu^2(z) \rangle$ will dictate the strength of coupling (e.g., related to Eq. 2.127). Furthermore, due to a resonance condition it will be found that only ocean structure with wavelengths equal to $k_n - k_m$ will enter the problem. This being the case, it is worthwhile to delve into the acoustic mode structure for deep and shallow-water environments where the mode approach is routinely applied.

Much can be learned about the structure of the modes and the character of the eigenvalues from an examination of the mode equation (Eq. 2.124). To simplify the analysis the mode functions are scaled by the density such that $\hat{\phi}_n = \phi_n / \sqrt{\rho_0}$, so that the mode equation becomes

$$\frac{d^2\hat{\phi}_n}{dz^2} + (\bar{k}_{eff}^2(z) - k_n^2)\hat{\phi}_n = 0, \tag{2.145}$$

where the effective background wavenumber is given by

$$\bar{k}_{eff}^2(z) = \frac{\omega^2}{\bar{c}^2} + \frac{1}{2}\left[\frac{1}{\rho_0} \frac{d^2\rho_0}{dz^2} - \frac{3}{2\rho_0^2} \left(\frac{d\rho_0}{dz} \right)^2 \right]. \tag{2.146}$$

From Eq. 2.145 it is recognized that the modes have a local vertical wavenumber given by

$$k_z(z) = \sqrt{\bar{k}_{eff}^2(z) - k_n^2}. \tag{2.147}$$

In depth regions where k_z is imaginary the mode functions will be evanescent, that is exponentially decaying, and in depth regions where k_z is real the modes

will be oscillating. The transition depth between oscillating and evanescent mode shape ($k_z = 0$) is called the mode turning depth denoted as $z^{\pm}$ where the $\pm$ refers to upper and lower turning points akin to the ray turning points. In most cases the effect of density on the vertical wavenumber is minimal, and from the turning point condition it is seen that $k_n/\omega = 1/c(z^{\pm})$. For the deep-water mid-latitude problem where the modes are trapped along a deep sound-channel axis, there are two turning points. In this case the upper turning point goes away when the mode becomes strongly surface interacting, a situation similar to the polar profile where all the modes are surface interacting. For the shallow-water case in which the sound speed in the bottom is larger than that in the water column, the lower turning point will be close to the water depth (independent of density), and there may or may not be an upper turning point depending on the degree that the mode is surface interacting.

At this point application of WKB methods are quite useful, and those not familiar with the technique should refer to Appendix B. Examining the mode equation (Eq. 2.145), one looks for solutions of the form $\phi_n \propto A(z)\mathrm{e}^{i\varphi(z)}$. The WKB envelope and phase functions are

$$A(z) \propto \frac{1}{\sqrt{k_z(z)}}, \tag{2.148}$$

$$\varphi(z) = \int_{z^-}^{z} k_z(z')\,dz', \tag{2.149}$$

where the phase function is defined only over the oscillatory modal depth region between the lower and upper turning points. The formal requirement for the validly of the WKB approximation is presented in Appendix B, but stated in another way the condition implies that over a vertical oscillation of the mode the sound-speed profile is not changing dramatically. As such, the WKB approximation generally improves as mode number increases. Note also that Eq. 2.148 tells us that away from the turning points the mode function envelope scales like $(c^2(z)/(c^2(z^{\pm}) - c^2(z)))^{1/4}$; thus it is expected that the mode functions will have amplitudes that slightly increase as the depth points move away from the sound-channel axis.

An important quantity is the vertical phase difference between the upper and lower turning points, termed the phase integral ($\varphi_n^{\pm}$),

$$\varphi_n^{\pm} = \int_{z_n^-}^{z_n^+} k_z(z)\,dz = \omega \int_{z_n^-}^{z_n^+} \sqrt{c^{-2}(z) - c^{-2}(z_n^{\pm})}\,dz. \tag{2.150}$$

In the evanescent regions of the mode, there are in fact exponentially growing solutions that can exist. To maintain a finite solution that is normalizable then

imposes the quantization conditions (Brekhovskikh and Lysanov, 1991)

$$\varphi_n^{\pm} = \pi(n - 1/2), \quad \text{two turning points,} \tag{2.151}$$

$$\varphi_n^{\pm} = \pi(n - 1/4), \quad \text{one turning point.} \tag{2.152}$$

For deep-water problems the two turning point case is more typical, except when the mode is strongly surface interacting or the profile is closer to the Arctic profile in which case only one, lower turning point exists. There are many useful applications of the quantization equations (Munk et al., 1995) that need not be discussed here. However, one practical use in the present case is in the estimate of the number of nonsurface interacting modes that fit into the waveguide (obtained by setting $z^+ = 0$ and solving for n). Here it is seen that the number of modes fitting into the waveguide scales linearly with the frequency. The number of modes will be an important numerical consideration when addressing mode-based fluctuation theories.

Some modes for the Munk canonical sound-speed profile for frequencies of 75 and 250 Hz are shown in Figure 2.12. Mode 1 is seen to be confined near the sound-channel axis, and as mode number increases the modes are seen to spread out vertically. Mode turning points are evident where the modes transition from oscillatory to exponentially decaying. The turning depths are a strong function of frequency. Clearly mode 1 will be influenced only by ocean sound-speed structure near the sound-channel axis. As mode number increases, it is found that modes are sensitive to the sound-speed structure near their turning points (more in Chapters 4 and 8).

Because the modal eigenvalues k_n are given by $\omega/c(z^{\pm})$ it is apparent that k_n decreases as n increases. That is to say as n increases the propagation can be considered in some senses to become more vertical. An effective mode grazing angle can be defined as

$$\tan\theta_g(n) = \frac{k_z(z_a)}{k_n} = c(z_n^{\pm})\sqrt{c^{-2}(z_a) - c^{-2}(z_n^{\pm})}, \tag{2.153}$$

and in this sense one can associate mode propagation with the corresponding ray with the same grazing angle and turning points. This association, often termed the "Ray-Mode Duality," has been known for some time and has been discussed at length by many authors (see Munk and Wunsch, 1983; Brekhovskikh and Lysanov, 1991, and references therein).

Figure 2.13 shows example modes for the canonical shallow-water sound-speed profile (Eq. 2.30) displayed in Figure 2.3. Here the acoustic frequencies are 400 and 1000 Hz. Because this profile has a mid-water sound-speed minimum, it is seen that mode 1 is confined near the depth of the axis. As mode number increases, the modes first become bottom interacting and then surface interacting. As before, the turning depths of the modes are a strong function of frequency.

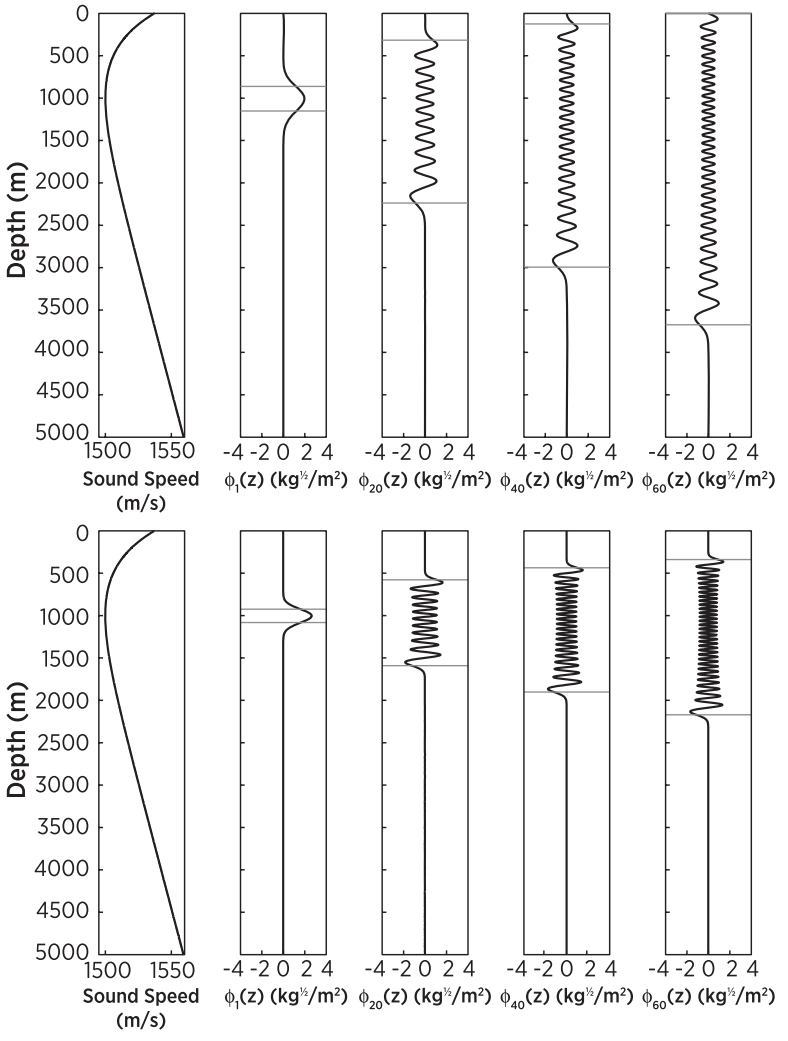

Figure 2.12. Mode functions for mode numbers 1, 20, 40, and 60 for the Munk canonical sound-speed profile shown at left. The top/bottom panels display modes for 75/250 Hz. Horizontal gray lines indicate upper and lower turning depths.

Next there is the matter of the eigenvalue spacing. It will be found in the theory of stochastic mode coupling that the strength of interaction between modes m and n will depend on the spectral strength of internal waves at the horizontal wavenumber $\kappa_{iw} = k_m - k_n = k_{mn}$. Because internal waves cause small-angle scattering, the strongest interactions will be between near neighbor modes. Thus it is useful to define the mode cycle distance

$$L_1(n) = \frac{2\pi}{k_n - k_{n-1}}, \tag{2.154}$$

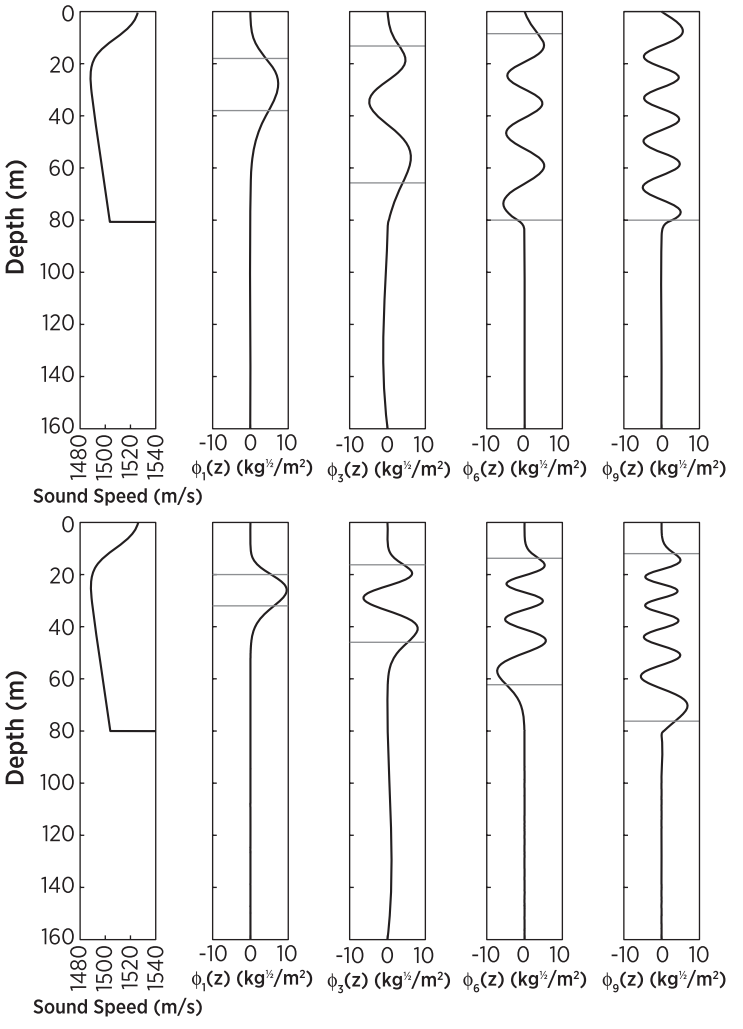

Figure 2.13. Mode functions for mode numbers 1, 3, 6, and 9 for the shallow-water canonical sound-speed profile shown at left. The bottom sound speed here is 1700 m/s and the bottom density is 1500 kg/m^3. The top/bottom panels display modes for 400/1000 Hz. Horizontal gray lines indicate upper and lower turning depths.

which physically represents the distance between nulls in the beat pattern between the neighboring modes n and $n-1$. This distance also has a correspondence with the ray double loop length for the ray with turning points $z_n^{\pm}$. Modes are expected to be most strongly influenced by internal waves with this horizontal wavelength. This is a modal manifestation of the ray loop resonance condition (Cornuelle and Howe, 1987; Munk et al., 1995), which will be discussed in Chapters 4 and 5. Because mode interactions do not drop to zero after neighboring modes, another

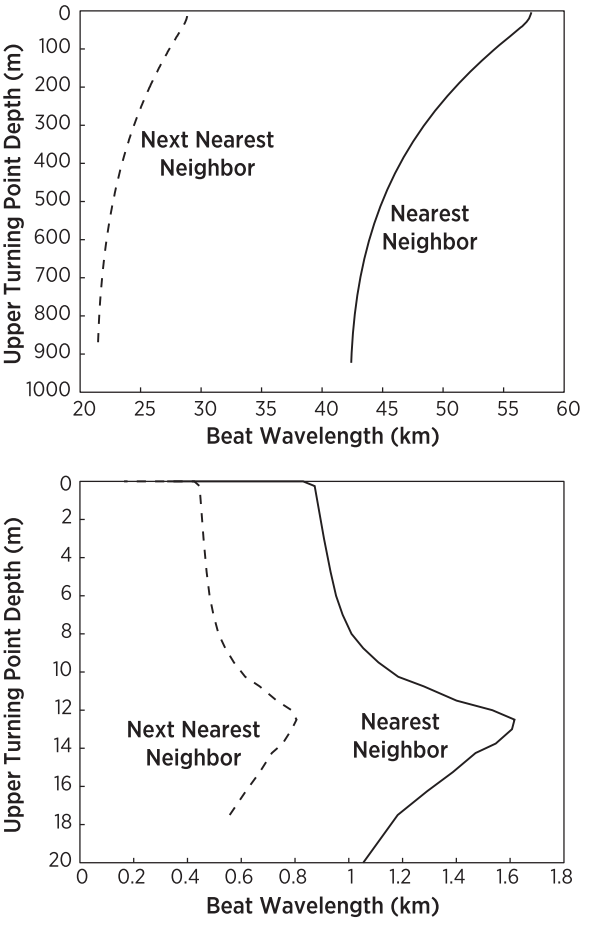

Figure 2.14. Nearest neighbor (solid) and next nearest neighbor (dash) beat wavelength ($L_1(n) = 2\pi/k_{n,n+1}$ and $L_2(n) = 2\pi/k_{n-1,n+1}$) for the Munk (top) and shallow-water canonical (bottom) sound-speed profiles.

useful quantity is the cycle distance of next nearest neighbor modes, that is

$$L_2(n) = \frac{2\pi}{k_{n+1} - k_{n-1}}. \tag{2.155}$$

This distance represents a harmonic of the ray loop distance. Figure 2.14 shows $L_1(n)$ and $L_2(n)$ plotted versus mode upper turning depth for the deep-water Munk profile and the canonical shallow-water profile previously discussed. As frequency changes specific modes move along the curves shown in Figure 2.14. The loop distances are indeed a function of mode number, so one expects the strength of acoustic scattering to also be a function of mode number. For the deep-water case the cycle distances are between 40 and 60 km for nearest neighbor interaction and they are between 20 and 30 km for next nearest neighbor interaction: These scales are ones with relatively high internal-wave spectral energy. On the other hand, for

the shallow-water case the nearest neighbor cycle distance is between 500 and 1600 m while the next nearest neighbor values are between 200 and 800 m. These scales have relatively low internal-wave spectral energy, and thus acoustic coupling due to internal waves is expected to be lower in shallow water.

Mid-Latitude Deep-Water Example

Figure 2.15 shows a mode calculation of a time front at 400-km range and the range evolution of single-frequency TL for propagation though the Munk canonical sound-speed profile. The mode-derived time front shows the same double accordion pattern displayed in the ray calculation (see Figure 2.5), but here the total acoustic field TL is shown. High intensity (low loss) is apparent where the time front branches connect. These are caustic regions. At the caustics, interference patterns are evident due to the interference between the two time front branches that join together. Similar interference is seen where the time front branches cross and in the final cut-off region where many branches are close together. If the bandwidth of the calculation were to be increased, the interference would correspondingly diminish. Away from caustics and interference regions, peak TL values along the time front branches in Figure 2.15 match with the ray estimates from Figure 2.8.

The modal interpretation of the time front is aided by a calculation of the mode phase and group speeds (see Figure 2.16). The mode phase speed, which is equal to the sound speed at the mode turning depth, is seen to mirror the upper part of the sound-speed profile. The mode group speed, on the other hand, rises gently from low modes with turning points near the axis and speeds near the axial speed (1500 m/s) to high modes with turning points near the surface and speeds near 1505 (m/s). This difference in group speed means that the early part of the time front arrival pattern is composed of high modes extending over a broad depth range of the water column, and the late arriving part of the pattern is composed of lower modes that are slower and confined in a narrower region around the sound-channel axis. A simple calculation based on these group speeds and the range of propagation predicts a time spread of roughly 0.85 s, which is indeed what is seen in Figure 2.15.

The single-frequency transmission loss fields shown in Figure 2.15 demonstrate refraction generated shadow zones, focusing regions, and a complex interference pattern consistent with the ray paths shown in Figure 2.4. Along the edges of shadow zones are caustic surfaces where the intensity is high. The degree to which acoustic energy penetrates into the shadow zone (i.e., the evanescent region of the caustic) depends on the acoustic frequency with higher frequencies (smaller wavelengths) showing less penetration. The spatial pattern of the interference pattern is also frequency dependent, with higher frequencies showing smaller separation between maxima and minima in the pattern.

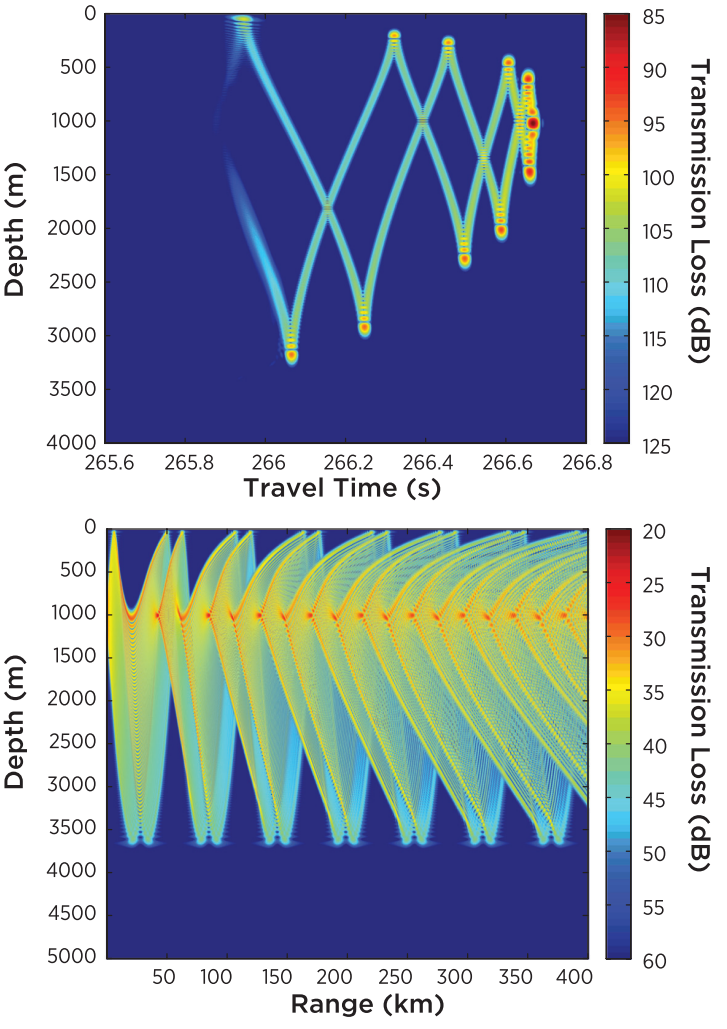

Figure 2.15. A mid-latitude time front at 400-km range (top) and the range evolution of single-frequency TL (bottom). For the calculations a Munk profile was used with a source depth of 1000-m (axial). For the time front 200 frequencies between 200 and 300 Hz were synthesized with a Hanning window to produce the front. A frequency of 250 Hz was used for the single-frequency calculation. For both the time front and single-frequency cases 200 normal modes were used. Full TL is shown for the time front, while TL without cylindrical spreading is displayed for the single-frequency.

When internal-wave-induced sound-speed perturbations are added to the problem, it is found that the early part of the time front, where the branches are well separated in time, remains relatively stable, with small deviations in wave front travel time and larger intensity variations along the front. However, in the late part of the arrival pattern, significant deviations are seen in the overall shape

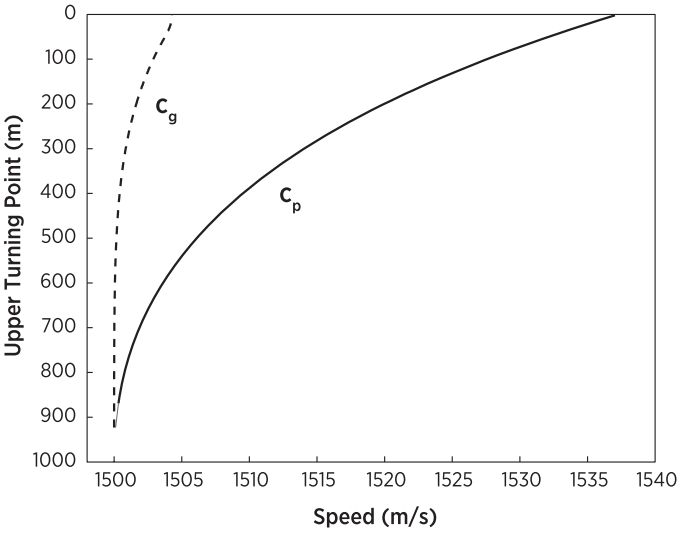

Figure 2.16. Modal phase (c_p) and group (c_g) speed for the Munk sound-speed profile as a function of mode upper turning depth.

of the front. Here separate branches of the front are overlapping resulting, in a complex interference pattern somewhat like the single-frequency example. For the entire time front, internal wave scattering will extend the ensonified region of the front in depth, leading to more sound in the shadow zones. For single frequencies both shadow zones and the interference pattern will be strongly affected by internal-wave-induced sound-speed perturbations. Sound will be scattered into the shadow zones, and the coherent interference pattern seen in Figure 2.15 will be replaced by a strongly fluctuating interference pattern.

Shallow-Water Example

Figure 2.17 shows a mode calculation of a time front at 20-km range, and the range evolution of single-frequency transmission loss. Unlike the deep-water mid-latitude case, the shallow-water time front bears little resemblance to an actual front as might be predicted from ray theory. The pattern instead resembles a series of mode arrivals, with the most energetic ones arriving first. In fact near travel times of 13.5 s, clearly separated arrivals for modes 7 and 8 are seen. This simple mode interpretation is one of the reasons why the theory of normal modes and not ray theory is used so extensively in shallow-water acoustics. As was the case for the deep-water example, the modal interpretation of the shallow-water time front is aided by a calculation of the horizontal phase and group speeds (see Figure 2.18). Here it is seen that the low modes with turning depths between 12 and 20 m have about the same group speeds, but as the mode number increases and the turning depths extend above 12 m, the group speed goes down precipitously.

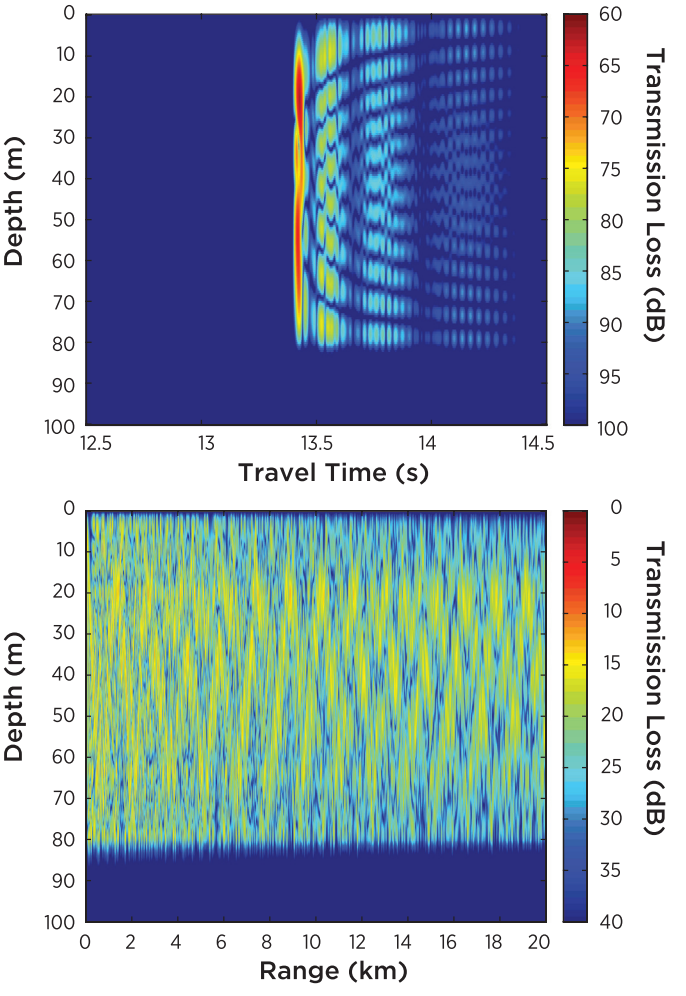

Figure 2.17. A shallow-water time front at 20-km range (top) and the range evolution of single-frequency transmission loss (bottom). For the calculations a canonical shallow-water profile (see Figure 2.3) was used with a source depth of 20 m (axial). For the time front 400 frequencies between 350 and 450 Hz were synthesized with a Hanning window to produce the front. A frequency of 400 Hz was used for the single-frequency calculation. For both the time front and single-frequency cases 18 normal modes were used. Full TL is shown for the time front, while TL without cylindrical spreading is displayed for the single-frequency. The bottom sound speed and density in this calculation are 1700 m/s and 1500 kg/m^3, and the bottom attenuation constant is 0.2 dB/λ.

Thus in this case the low modes get down range fastest, and the higher modes trail behind. The low modes are also the most energetic because they are trapped in the gentle sound-speed minimum and therefore do not interact strongly with the lossy seabed. It is not generally the case that the low modes have such small

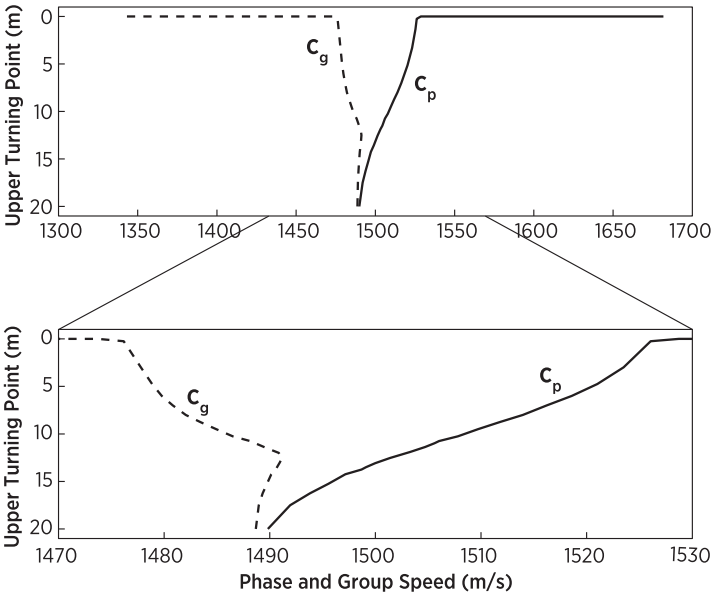

Figure 2.18. Modal phase (c_p) and group (c_g) speed for the canonical shallow-water sound-speed profile (see Figure 2.3) as a function of mode upper turning depth.

bottom interaction. A useful interpretation of this arrival pattern is in terms of the mode-pulses described in Eq. 2.142.

The range evolution of the single-frequency transmission loss field in Figure 2.17 shows significantly less structure than the corresponding deep-water case. In the shallow water, a complicated interference pattern is present over the entire spatial region, and there are no clear shadow zones, caustic surfaces, or focusing regions. As range increases, the interference pattern is seen to simplify significantly. This effect is due to the attenuation of the higher modes from bottom interaction, often termed "mode stripping," and thus at longer range the interference pattern is primarily due to the low modes.

When internal waves are included, shallow-water acoustic fields are seen to change significantly due to mode coupling and cross mode decorrelation or loss of coherence. Intensity patterns can shift dramatically as coupling transfers acoustic energy back and forth between low and high modes, and modal phase randomization occurs. The result of these two effects is that the coherent mode arrival pattern seen in the shallow-water time front is washed out, leaving a complex interference pattern, not unlike the single-frequency example. In the single-frequency case mode coupling and phase randomization lead to a highly fluctuating multimode interference pattern.

Appendix A Green's Functions and the Fresnel Zone

Consider the second-order ray tube Green's function equation that follows the ray $z_r(x)$,

$$\left(\frac{d^2}{dx^2} + V''(x)\right)g(x,x') = \delta(x-x'). \tag{A.1}$$

For fixed end points ($x = 0$ and $x = R$) one can write the two solutions to this second-order equation as

$$\xi_1(x) \;\rightarrow\quad 0 < x < x', \quad \xi_1(0) = 0, \quad g^{<}(x,x') = A\xi_1(x), \tag{A.2}$$

$$\xi_2(x) \;\rightarrow\quad x' < x < R, \quad \xi_2(R) = 0, \quad g^{>}(x,x') = B\xi_2(x). \tag{A.3}$$

The solutions must match at $x = x'$, giving the result

$$A\xi_1(x') = B\xi_2(x'). \tag{A.4}$$

Next one integrates Eq. A.1 around the delta function position x', giving

$$\int_{x'-\epsilon}^{x'+\epsilon}\left(\frac{d^2}{dx^2} + V''(x)\right)g(x,x')\,dx = 1. \tag{A.5}$$

Here the second term in the integral is of order ϵ thus it can be ignored, leading to the result,

$$\frac{d}{dx}g(x,x')\Big|_{x'-\epsilon}^{x'+\epsilon} = \left[\frac{d}{dx}g^{>}(x,x') - \frac{d}{dx}g^{<}(x,x')\right] = 1. \tag{A.6}$$

So the Green's function slope discontinuity at $x = x'$ is unity. Combining Eq. A.4 and A.6 the expressions for the constants A and B are

$$A = \frac{\xi_2(x')}{W(x')}, \qquad B = \frac{\xi_1(x')}{W(x')}, \tag{A.7}$$

where

$$W(x') = \text{Wronskian} = \xi_1\frac{d\xi_2}{dx} - \xi_2\frac{d\xi_1}{dx}. \tag{A.8}$$

It can also be shown that W = constant. Both ξ_1 and ξ_2 satisfy the homogeneous equations

$$\left(\frac{d^2}{dx^2} + V''(x)\right)\xi_1 = 0, \qquad \left(\frac{d^2}{dx^2} + V''(x)\right)\xi_2 = 0. \tag{A.9}$$

Thus multiplying the first equation by ξ_2 and the second equation by ξ_1 and subtracting one gets

$$\xi_2 \frac{d^2}{dx^2}\xi_1 - \xi_1 \frac{d^2}{dx^2}\xi_2 = \frac{dW}{dx} = 0, \tag{A.10}$$

hence demonstrating that the Wronskian is constant. Thus the final expression for the Green's function can be given:

$$g^{<}(x,x') = \frac{\xi_1(x)\xi_2(x')}{W}, \qquad g^{>}(x,x') = \frac{\xi_1(x')\xi_2(x)}{W}. \tag{A.11}$$

Note that the Fresnel zone given by Eq. 2.89 can be expressed in terms of the Green's function such that $R_f^2(x) = \lambda g(x,x)$.

The calculation of the Fresnel zone requires ray tube functions ξ_1 and ξ_2 that satisfy the boundary conditions at the source and the receiver. In practice these ray tube functions are constructed from two other solutions ξ_{IV1} and ξ_{IV2} that satisfy a specific initial value problem. For the initial and boundary value problems consider the following:

$$\xi_{IV1}(0) = 0 \;\; \xi_{IV1}{}'(0) = 1, \xi_{IV2}(0) = 1 \;\; \xi_{IV2}{}'(0) = 0, \tag{A.12}$$

$$\xi_1(0) = 0 \;\; \xi_1(R) = 1, \xi_2(0) = 1 \;\; \xi_2(R) = 0, \tag{A.13}$$

and so combining these solutions gives

$$\xi_1 = \frac{\xi_{IV1}(x)}{\xi_{IV1}(R)}, \xi_2 = \xi_{IV2}(x) - \xi_{IV1}(x)\frac{\xi_{IV2}(R)}{\xi_{IV1}(R)}. \tag{A.14}$$

Here it is chosen to evaluate the Wronskian W at $x = 0$ which gives us the result $W(x=0) = -1/\xi_{IV1}(R)$. Thus the Fresnel zone is given by

$$R_f^2(x) = \lambda \xi_1(x)\xi_2(x)\xi_{IV1}(R). \tag{A.15}$$

It is important to note that there are problems if the receiver is near a caustic, that is $\xi_{IV1}(R) = 0$.

Examples

Consider the case of a polar sound-speed profile given by $c = c_0(1 + \gamma_a z)$, then $V \simeq \gamma_a z$ and $V'' \simeq 0$. This case also applies to the constant sound-speed profile. The ray tube equation therefore is the form $d^2\xi/dx^2 = 0$, which has solutions $\xi = Ax + B$. The ray tube functions are then given by

$$\xi_{IV1}(x) = x, \qquad \xi_1(x) = \frac{x}{R}, \qquad \xi_2(x) = \frac{(R-x)}{R}, \tag{A.16}$$

thus giving the Fresnel zone

$$R_f^2(x) = \lambda \xi_1(x)\xi_2(x)\xi_{IV1}(R) = \lambda \frac{x(R-x)}{R}. \tag{A.17}$$

This is the point source Fresnel zone for a constant linear profile, and for a constant background sound speed.

Next consider a quadratic sound-speed profile such as one might encounter for a mid-latitude sound-speed profile near the channel axis. Here V'' is roughly a constant, and the ray tube functions are

$$\xi_{IV1}(x) = \frac{\sin K_a x}{K_a}, \qquad \xi_1(x) = \frac{\sin K_a x}{\sin K_a R}, \qquad \xi_2(x) = \sin K_a(R-x), \tag{A.18}$$

where $K_a = 2\pi/R_a = \sqrt{V''}$ is the horizontal wavenumber of the sinusoidal ray loop with double loop range R_a. The Fresnel zone is thus

$$R_f^2(x) = \lambda \left| \frac{\sin K_a x \ \sin K_a(R-x)}{K_a \sin K_a R} \right|. \tag{A.19}$$

For the Munk canonical profile at the axis $K_a = \sqrt{2\gamma_a/B}$.

Appendix B WKB Modes

WKB analysis of the vertical mode equations for both acoustic and internal waves is essential to the clear exposition of this book. The acoustic and internal wave mode equations (Eqs. 2.124 and 3.26) can be cast in a general form given by

$$\frac{d^2B}{dz^2} + k_z^2(z)B = 0, \tag{B.1}$$

where k_z is considered to be real. For the deep-water acoustic problem, water-borne modes obeying Eq. 2.145 clearly fit this general form. When acoustic bottom interactions are involved, Eq. 2.124 can be mapped to the general form by the substitution $\hat{\phi}_n = \phi_n / \sqrt{\rho_0}$.

The WKB method consists of examining solutions to the mode equation that are of the form $B(z) \propto A(z)e^{i\varphi(z)}$. Plugging this form into the mode equation yields two equations from the real and imaginary parts, written

$$\frac{d^2A}{dz^2} - A\left(\frac{d\varphi}{dz}\right)^2 + k_z^2(z)A = 0, \tag{B.2}$$

$$A\frac{d^2\varphi}{dz^2} + 2\frac{dA}{dz}\frac{d\varphi}{dz} = 0. \tag{B.3}$$

The solution to the second equation is given by

$$\frac{d\varphi}{dz} = \frac{C}{A^2}, \tag{B.4}$$

where C is an integration constant. Substituting this equation into the first yields

$$\frac{1}{A}\frac{d^2A}{dz^2} - \frac{C^2}{A^4} + k_z^2(z) = 0. \tag{B.5}$$

From a local plane wave approximation clearly $k_z(z) = d\varphi/dz$. Thus it is apparent that the last two terms in Eq. B.5 are proportional to k_z^2, while the first term is roughly independent of k_z. If the mode phase φ is changing more rapidly than the envelope function $A(z)$, then the first term can be ignored. Formally this is the condition $k_z^2(z) >> (1/A)d^2A/dz^2$. This case applies mores readily to higher order modes. The WKB envelope and phase functions are therefore

$$A(z) \propto \frac{1}{\sqrt{k_z(z)}}, \tag{B.6}$$

$$\varphi(z) = \int_{z^-}^{z} k_z(z')\,dz', \tag{B.7}$$

where the mode phase has been written relative to a lower turning point z^- with $k_z(z^-) = 0$. Clearly in depth regions where k_z is complex, the modes will be evanescent and this analysis will not apply. Also near turning points where $k_z(z) = 0$ special treatment is required (i.e., Airy Solutions (see Garrett and Munk, 1972)).